3 Solar radiation and the global energy budget

Learning objectives
When you have read this chapter you will:

- Know the characteristics of solar radiation and the electromagnetic spectrum,
- Know the effects of the atmosphere on solar and terrestrial radiation,
- Understand the cause of the atmospheric greenhouse effect,
- Understand the earth's heat budget and the importance of horizontal transfers of energy as sensible and latent heat.

This chapter describes how radiation from the sun enters the atmosphere and reaches the surface. The effects on solar radiation of absorbing gases and the scattering effects of aerosols are examined. Then terrestrial long-wave (infra-red) radiation is discussed in order to explain the radiation balance. At the surface, an energy balance exists due to the additional transfers of sensible and latent heat to the atmosphere. The effects of heating on surface temperature characteristics are then presented.

A SOLAR RADIATION

The source of the energy injected into our atmosphere is the sun, which is continually shedding part of its mass by radiating waves of electromagnetic energy and high-energy particles into space. This constant emission represents all the energy available to the earth (except for a small amount emanating from the radioactive decay of earth minerals). The amount of energy received at the top of the atmosphere is affected by four factors: solar output, the sun–earth distance, the altitude of the sun, and day length.

1 Solar output

Solar energy originates from nuclear reactions within the sun's hot core (16×10^6 K), and is transmitted to the sun's surface by radiation and hydrogen convection. Visible solar radiation (light) comes from a 'cool' (~6000 K) outer surface layer called the *photosphere*. Temperatures rise again in the outer chromosphere (10,000 K) and corona (10^6 K), which is continually expanding into space. The outflowing hot gases (plasma) from the sun, referred to as the *solar wind* (with a speed of 1.5×10^6 km hr^{-1}), interact with the earth's magnetic field and upper atmosphere. The earth intercepts both the normal electromagnetic radiation and energetic particles emitted during solar flares.

The sun behaves virtually as a *black body*; i.e. it absorbs all energy received and in turn radiates energy

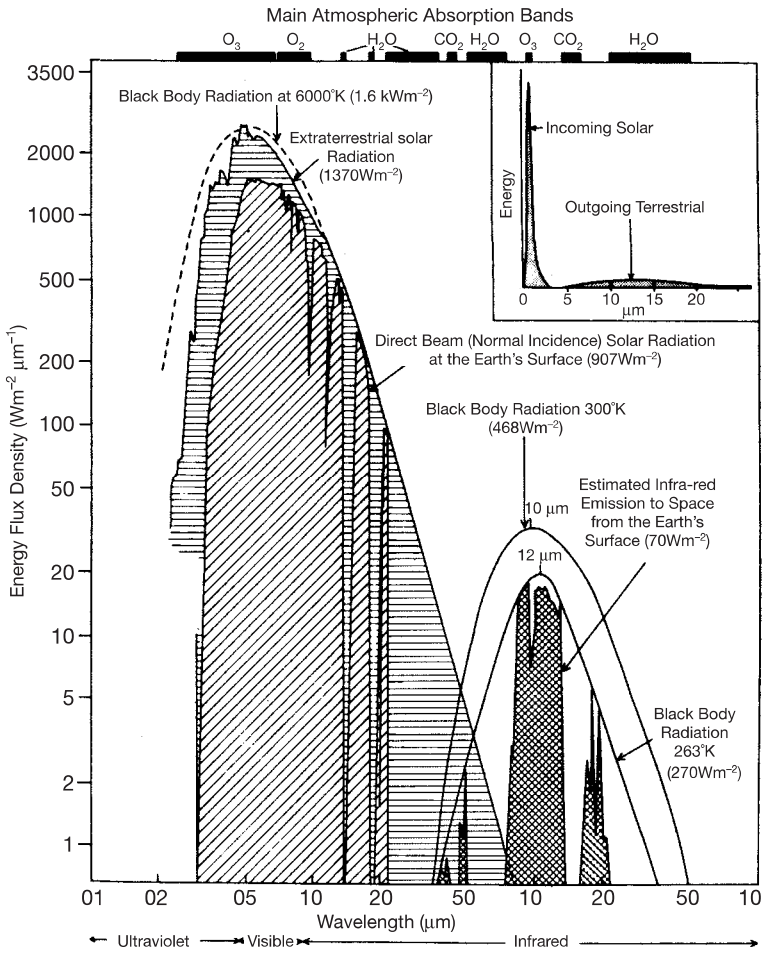

Figure 3.1 Spectral distribution of solar and terrestrial radiation, plotted logarithmically, together with the main atmospheric absorption bands. The cross-hatched areas in the infra-red spectrum indicate the 'atmospheric windows' where radiation escapes to space. The black-body radiation at 6000 K is that proportion of the flux which would be incident on the top of the atmosphere. The inset shows the same curves for incoming and outgoing radiation with the wavelength plotted arithmetically on an arbitrary vertical scale.

Source: Mostly after Sellers (1965).

at the maximum rate possible for a given temperature. The energy emitted at a particular wavelength by a perfect radiator of given temperature is described by a relationship due to Max Planck. The black-body curves in Figure 3.1 illustrate this relationship. The area under each curve gives the total energy emitted by a black body (F); its value is found by integration of Planck's equation, known as Stefan's Law:

$$F = \sigma T^4$$

where $\sigma = 5.67 \times 10^{-8}$ W m^{-2} K^{-4} (the Stefan–Boltzmann constant), i.e. the energy emitted is proportional to the fourth power of the absolute temperature of the body (T).

The total solar output to space, assuming a temperature of 5760 K for the sun, is 3.84×10^{26}W, but only a tiny fraction of this is intercepted by the earth, because the energy received is inversely proportional to the square of the solar distance (150 million km). The energy received at the top of the atmosphere on a surface perpendicular to the solar beam for mean solar distance is termed the *solar constant* (see Note 1). Satellite measurements since 1980 indicate a value of about 1366 W m^{-2}, with an absolute uncertainty of about $\pm$2 W m^{-2}. Figure 3.1 shows the wavelength range of solar (short-wave) radiation and the infra-red (long-wave) radiation emitted by the earth and atmosphere. For solar radiation, about 7 per cent is ultraviolet (0.2-0.4 μm), 41 per cent visible light (0.4–0.7 μm) and 52 per cent near-infra-red (>0.7 μm); (1 μm = 1 micrometre = 10^{-6} m). The figure illustrates the black-body radiation curves for 6000 K at the top of the atmosphere (which slightly exceeds the observed extraterrestrial radiation), for 300 K, and for 263 K. The

mean temperature of the earth's surface is about 288 K (15°C) and of the atmosphere about 250 K (–23°C). Gases do not behave as black bodies, and Figure 3.1 shows the absorption bands in the atmosphere, which cause its emission to be much less than that from an equivalent black body. The wavelength of maximum emission (λ_{max}) varies inversely with the absolute temperature of the radiating body:

$$\lambda_{max} = \frac{2897}{T} 10^{-6} \text{ m (Wien's Law)}$$

Thus solar radiation is very intense and is mainly shortwave between about 0.2 and 4.0 μm, with a maximum (per unit wavelength) at 0.5 μm because $T \sim 6000$ K. The much weaker terrestrial radiation with $T \approx 280$ K has a peak intensity at about 10 μm and a range from about 4 to 100 μm.

The solar constant undergoes small periodic variations of just over 1 Wm^{-2} related to sunspot activity. Sunspot number and positions change in a regular manner, known as sunspot cycles. Satellite measurements during the latest cycle show a small decrease in solar output as sunspot number approached its *minimum*, and a subsequent recovery. *Sunspots* are dark (*i.e.* cooler) areas visible on the sun's surface. Although sunspots are cool, bright areas of activity known as *faculae* (or *plages*), that have higher temperatures, surround them. The net effect is for solar output to vary in parallel with the number of sunspots. Thus the solar 'irradiance' decreases by about 1.1 Wm^{-2} from sunspot maximum to minimum. Sunspot cycles have wavelengths averaging 11 years (the Schwabe cycle, varying between 8 and 13 years), the 22-year (Hale) magnetic cycle, much less importantly 37.2 years (18.6 years – the luni–solar oscillation), and 88 years (Gleissberg). Figure 3.2 shows the estimated variation of sunspot activity since 1610. Between the thirteenth and eighteenth centuries sunspot activity was generally low, except during AD 1350–1400 and 1600–1645. Output within the ultraviolet part of the spectrum shows considerable variability, with up to twenty times more ultraviolet radiation emitted at certain wavelengths during a sunspot maximum than a minimum.

How to translate sunspot activity into solar radiation and terrestrial temperatures is a matter of some dispute. It has been suggested that the sun is more active when the sunspot cycle length is short, but this is disputed. However, anomalies of temperature over northern hemisphere land areas do correlate inversely with cycle length between 1860 and 1985. Prolonged time-spans of sunspot minima (e.g. AD 1645–1715, the Maunder Minimum) and maxima (e.g. 1895–1940 and post-1970) produce measurable global cooling and warming, respectively. Solar radiation may have been reduced by 0.25 per cent during the Maunder Minimum. It is suggested that almost three-quarters of the variations in global temperature between 1610 and 1800 were attributable to fluctuations in solar radiation and during the twentieth century there is evidence for a modest contribution from solar forcing. Shorter term relationships are more difficult to support, but mean annual temperatures have been correlated with the combined 10 to 11 and 18.6-year solar cycles. Assuming that the earth behaves as a black body, a persistent anomaly of 1 per cent in the solar constant could change the effective mean temperature of the earth's surface by as much as 0.6°C. However, the observed fluctuations of about 0.1 per cent would change the mean global temperature by ≤0.06°C (based on calculations of radiative equilibrium).

2 Distance from the sun

The annually changing distance of the earth from the sun produces seasonal variations in solar energy received by the earth. Owing to the eccentricity of the earth's orbit around the sun, the receipt of solar energy on a surface normal to the beam is 7 per cent more on 3 January at the perihelion than on 4 July at the aphelion (Figure 3.3). In theory (that is, discounting the interposition of the atmosphere and the difference in degree of conductivity between large land and sea masses), this difference should produce an increase in the effective January world surface temperatures of about 4°C over those of July. It should also make northern winters warmer than those in the southern hemisphere, and southern summers warmer than those in the northern hemisphere. In practice, atmospheric heat circulation and the effects of continentality mask this global tendency, and the actual seasonal contrast between the hemispheres is reversed. Moreover, the northern summer half-year (21 March to 22 September) is five days longer than the austral summer (22 September to 21 March). This difference slowly changes; about 10,000 years ago the aphelion occurred in the northern hemisphere winter, and northern summers received 3 to

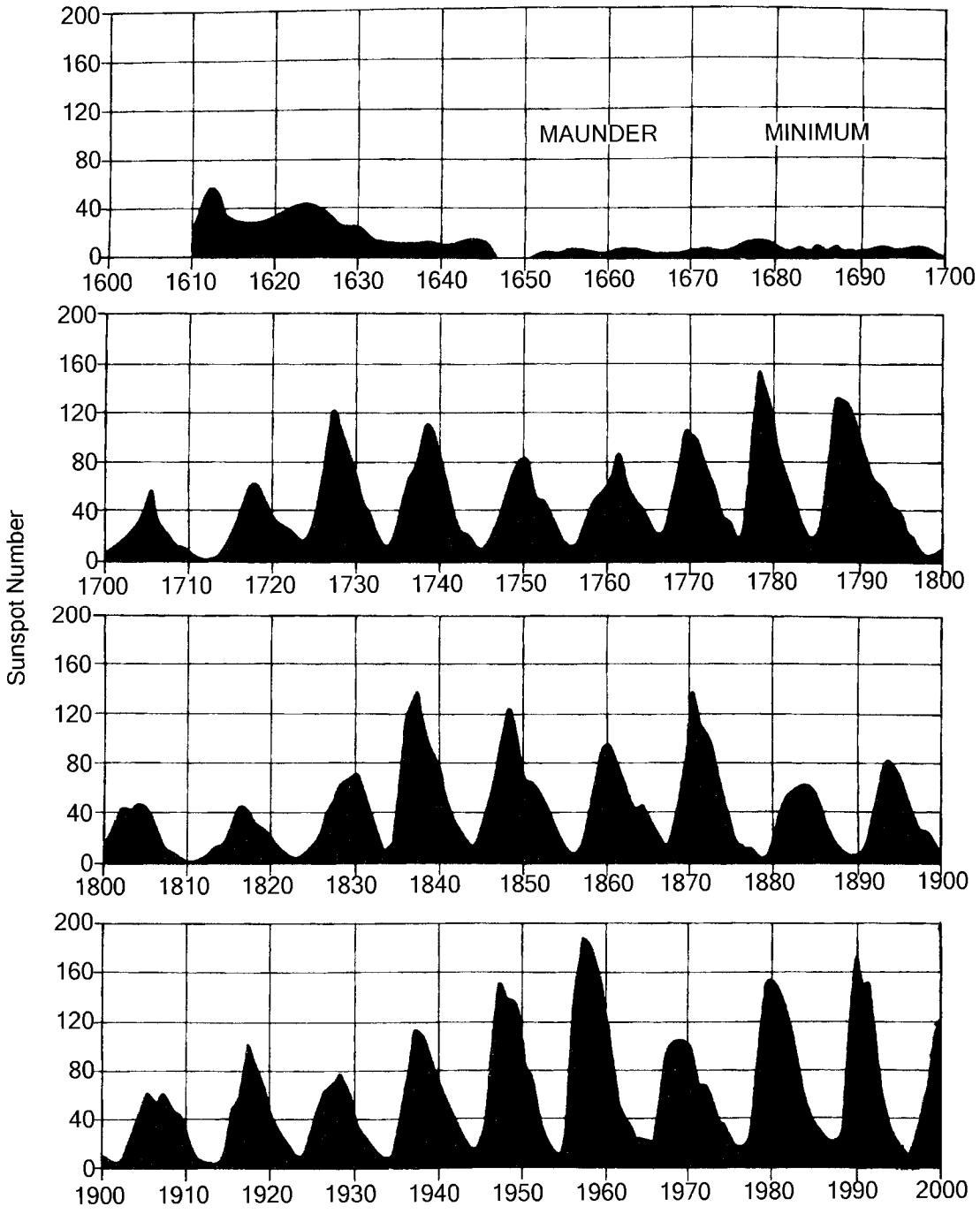

Figure 3.2 Yearly sunspot numbers for the sun's visible surface for the period 1700 to 2000.

Sources: Reproduced by courtesy of the National Geophysical Data Center, NOAA, Boulder, CO. Data before AD 1700 courtesy of Foukal (1990) and *Scientific American*.

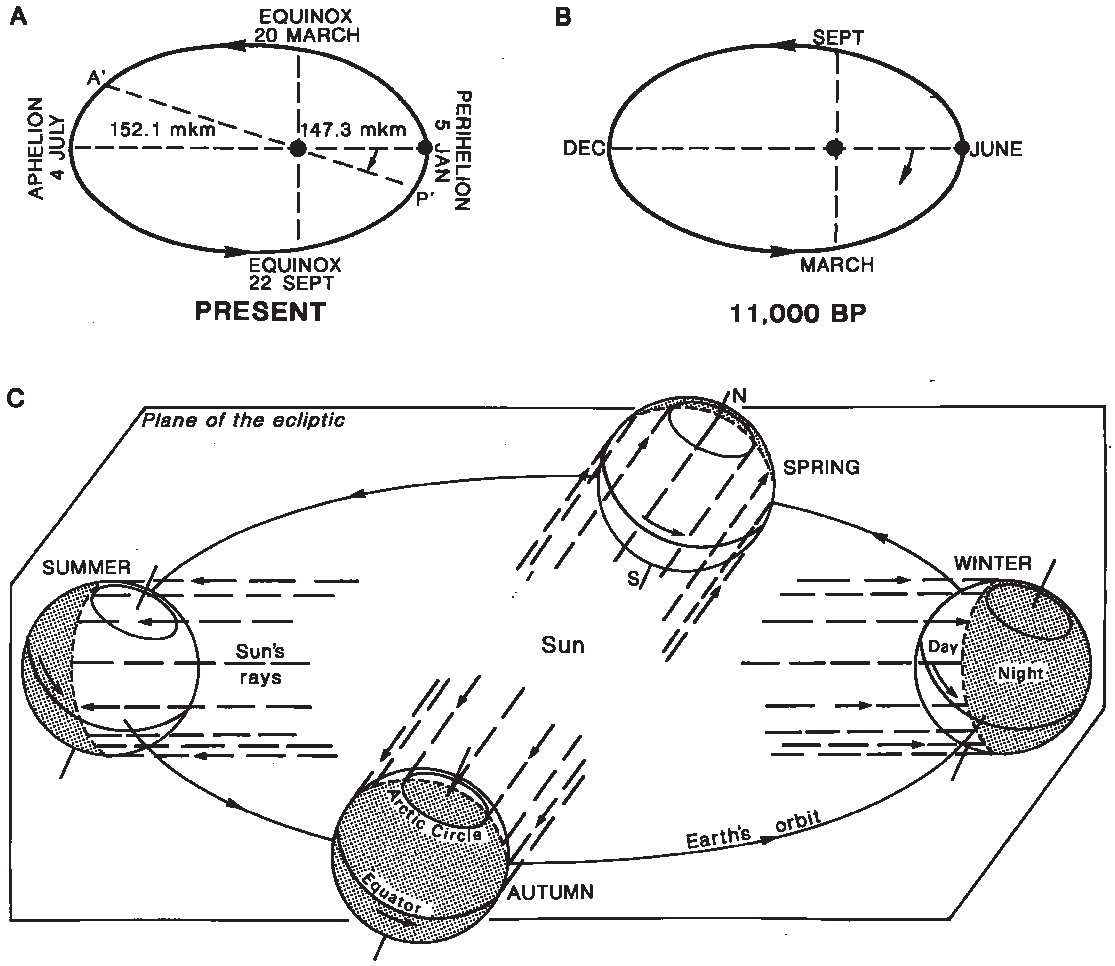

Figure 3.3 Perihelion shifts. (A) The present timing of perihelion. (B) The direction of its shift and the situation at 11,000 years BP. (C) The geometry of the present seasons (northern hemisphere).

Source: Partly after Strahler (1965).

4 per cent more radiation than today (Figure 3.3B). This same pattern will return about 10,000 years from now.

Figure 3.4 graphically illustrates the seasonal variations of energy receipt with latitude. Actual amounts of radiation received on a horizontal surface outside the atmosphere are given in Table 3.1. The intensity on a horizontal surface (I_h) is determined from:

$$I_h = I_0 \sin d$$

where I_0 = the solar constant and d = the angle between the surface and the solar beam.

3 Altitude of the sun

The altitude of the sun (i.e. the angle between its rays and a tangent to the earth's surface at the point of observation) also affects the amount of solar radiation received at the surface of the earth. The greater the sun's altitude, the more concentrated is the radiation intensity per unit area at the earth's surface and the shorter is the path length of the beam through the atmosphere, which decreases the atmospheric absorption. There are, in addition, important variations with solar altitude of the proportion of radiation reflected by the surface, particularly in the case of a water surface (see B.5, this

Table 3.1 Daily solar radiation on a horizontal surface outside the atmosphere: W m^{-2}.

Date	*90°N*	*70*	*50*	*30*	*0*	*30*	*50*	*70*	*90°S*
21 Dec	0	0	86	227	410	507	514	526	559
21 Mar	0	149	280	378	436	378	280	149	0
22 June	524	492	482	474	384	213	80	0	0
23 Sept	0	147	276	373	430	372	276	147	0

Source: After Berger (1996).

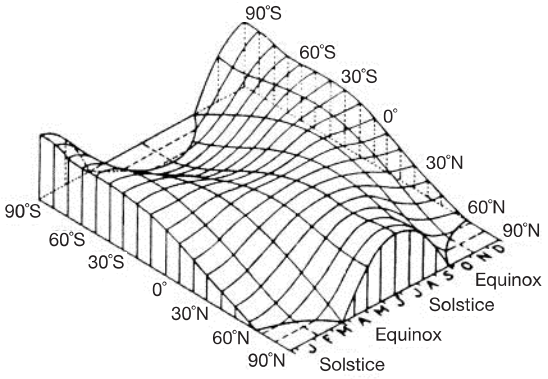

Figure 3.4 The variations of solar radiation with latitude and season for the whole globe, assuming no atmosphere. This assumption explains the abnormally high amounts of radiation received at the poles in summer, when daylight lasts for twenty-four hours each day.

Source: After W. M. Davis.

chapter). The principal factors that determine the sun's altitude are, of course, the latitude of the site, the time of day and the season (see Figure 3.3). At the June solstice, the sun's altitude is a constant 23½° throughout the day at the North Pole and the sun is directly overhead at noon at the Tropic of Cancer (23½°N).

4 Length of day

The length of daylight also affects the amount of radiation that is received. Obviously, the longer the time the sun shines the greater is the quantity of radiation that a given portion of the earth will receive. At the equator, for example, the day length is close to 12 hours in all months, whereas at the poles it varies between 0 and 24 hours from winter (polar night) to summer (see Figure 3.3).

The combination of all these factors produces the pattern of receipt of solar energy at the top of the atmosphere shown in Figure 3.4. The polar regions receive their maximum amounts of solar radiation during their summer solstices, which is the period of continuous day. The amount received during the December solstice in the southern hemisphere is theoretically greater than that received by the northern hemisphere during the June solstice, due to the previously mentioned elliptical path of the earth around the sun (see Table 3.1). The equator has two radiation maxima at the equinoxes and two minima at the solstices, due to the apparent passage of the sun during its double annual movement between the northern and southern hemispheres.

B SURFACE RECEIPT OF SOLAR RADIATION AND ITS EFFECTS

1 Energy transfer within the earth–atmosphere system

So far, we have described the distribution of solar radiation as if it were all available at the earth's surface. This is, of course, unrealistic because of the effect of the atmosphere on energy transfer. Heat energy can be transferred by three mechanisms:

1 *Radiation*: Electromagnetic waves transfer energy (both heat and light) between two bodies, without the necessary aid of an intervening material medium, at a speed of 300×10^6 m s^{-1} (i.e. the speed of light). This is so with solar energy through space, whereas the earth's atmosphere allows the passage of radiation only at certain wavelengths and restricts that at others.

Radiation entering the atmosphere may be absorbed in certain wavelengths by atmospheric gases but, as shown in Figure 3.1, most short-wave radiation is transmitted without absorption. Scattering

occurs if the direction of a photon of radiation is changed by interaction with atmospheric gases and aerosols. Two types of scattering are distinguished. For gas molecules smaller than the radiation wavelength (λ), *Rayleigh scattering* occurs in all directions (i.e. it is *isotropic*) and is proportional to ($1/\lambda^4$). As a result, the scattering of blue light ($\lambda \sim 0.4$ μm) is an order of magnitude (i.e. $\times 10$) greater than that of red light ($\lambda \sim 0.7$ μm), thus creating the daytime blue sky. However, when water droplets or aerosol particles, with similar sizes (0.1–0.5 μm radius) to the radiation wavelength are present, most of the light is scattered forward. This *Mie scattering* gives the greyish appearance of polluted atmospheres.

Within a cloud, or between low clouds and a snow-covered surface, radiation undergoes multiple scattering. In the latter case, the 'white-out' conditions typical of polar regions in summer (and mid-latitude snowstorms) are experienced, when surface features and the horizon become indistinguishable.

2 *Conduction*: By this mechanism, heat passes through a substance from a warmer to a colder part through the transfer of adjacent molecular vibrations. Air is a poor conductor so this type of heat transfer is negligible in the atmosphere, but it is important in the ground. The thermal conductivity increases as the water content of a given soil increases and is greater in a frozen soil than in an unfrozen one.

3 *Convection*: This occurs in fluids (including gases) that are able to circulate internally and distribute heated parts of the mass. It is the chief means of atmospheric heat transfer due to the low viscosity of air and its almost continual motion. *Forced convection* (mechanical turbulence) occurs when eddies form in airflow over uneven surfaces. In the presence of surface heating, *free* (thermal) *convection* develops.

Convection transfers energy in two forms. The first is the *sensible heat* content of the air (called enthalpy by physicists), which is transferred directly by the rising and mixing of warmed air. It is defined as c_pT, where T is the temperature and c_p (= 1004 J kg^{-1} K^{-1}) is the specific heat at constant pressure (the heat absorbed by unit mass for unit temperature increase). Sensible heat is also transferred by conduction. The second form of energy transfer by convection is indirect, involving *latent heat*. Here, there is a phase change but no temperature change. Whenever water is converted into water vapour by evaporation (or boiling), heat is required. This is referred to as the latent heat of vaporization (L). At 0°C, L is 2.50×10^6 J kg^{-1} of water. More generally,

$$L\ (10^6\ J\ kg^{-1}) = (2.5 - 0.00235T)$$

where T is in °C. When water condenses in the atmosphere (see Chapter 4D), the same amount of latent heat is given off as is used for evaporation *at the same temperature*. Similarly, for melting ice at 0°C, the latent heat of fusion is required, which is 0.335×10^6 J kg^{-1}. If ice evaporates without melting, the latent heat of this sublimation process is 2.83×10^6 J kg^{-1} at 0°C (i.e. the sum of the latent heats of melting and vaporization). In all of these phase changes of water there is an energy transfer. We discuss other aspects of these processes in Chapter 4.

2 Effect of the atmosphere

Solar radiation is virtually all in the short-wavelength range, less than 4 μm (see Figure 3.1). About 18 per cent of the incoming energy is absorbed directly by ozone and water vapour. Ozone absorption is concentrated in three solar spectral bands (0.20–0.31, 0.31–0.35 and 0.45–0.85 μm), while water vapour absorbs to a lesser degree in several bands between 0.9 and 2.1 μm (see Figure 3.1). Solar wavelengths shorter than 0.285 μm scarcely penetrate below 20 km altitude, whereas those >0.295 μm reach the surface. Thus the 3 mm (equivalent) column of stratospheric ozone attenuates ultraviolet radiation almost entirely, except for a partial window around 0.20 μm, where radiation reaches the lower stratosphere. About 30 per cent of incoming solar radiation is immediately reflected back into space from the atmosphere, clouds and the earth's surface, leaving approximately 70 per cent to heat the earth and its atmosphere. The surface absorbs almost half of the incoming energy available at the top of the atmosphere and re-radiates it outward as long (infra-red) waves of greater than 3 μm (see Figure 3.1). Much of this re-radiated long-wave energy is then absorbed by the water vapour, carbon dioxide and ozone in the atmosphere, the rest escaping through atmospheric *windows* back into outer space, principally between 8 and 13 μm (see Figure 3.1). This retention of energy by the atmosphere is vital to most life forms, since otherwise the average

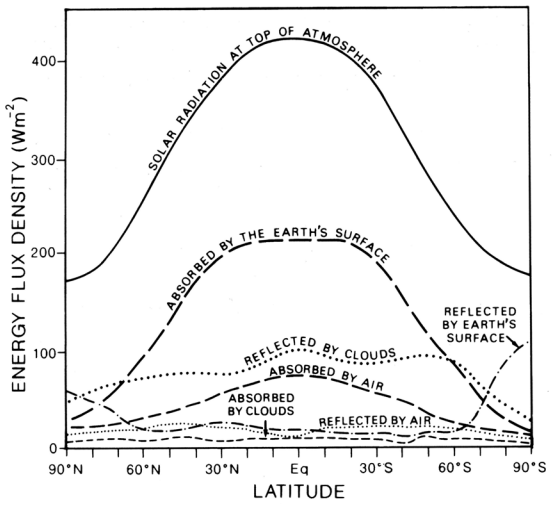

Figure 3.5 The average annual latitudinal disposition of solar radiation in W m^{-2}. Of 100 per cent radiation entering the top of the atmosphere, about 20 per cent is reflected back to space by clouds, 3 per cent by air (plus dust and water vapour), and 8 per cent by the earth's surface. Three per cent is absorbed by clouds, 18 per cent by the air, and 48 per cent by the earth.

Source: After Sellers (1965).

temperature of the earth's surface would fall by some 40°C!

The atmospheric scattering, noted above, gives rise to *diffuse* (or sky) radiation and this is sometimes measured separately from the direct beam radiation. On average, under cloud-free conditions the ratio of diffuse to total (or global) solar radiation is about 0.15–0.20 at the surface. For average cloudiness, the ratio is about 0.5 at the surface, decreasing to around 0.1 at 4 km, as a result of the decrease in cloud droplets and aerosols with altitude. During a total solar eclipse, experienced over much of western Europe in August 1999, the elimination of direct beam radiation caused diffuse radiation to drop from 680 W m^{-2} at 10.30 a.m. to only 14 W m^{-2} at 11.00 a.m. at Bracknell in southern England.

Figure 3.5 illustrates the relative roles of the atmosphere, clouds and the earth's surface in reflecting and absorbing solar radiation at different latitudes. (A more complete analysis of the heat budget of the earth–atmosphere system is given in D, this chapter.)

3 Effect of cloud cover

Thick and continuous cloud cover forms a significant barrier to the penetration of radiation. The drop in surface temperature often experienced on a sunny day when a cloud temporarily cuts off the direct solar radiation illustrates our reliance upon the sun's radiant energy. How much radiation is actually reflected by clouds depends on the amount of cloud cover and its thickness (Figure 3.6). The proportion of incident radiation that is reflected is termed the *albedo*, or reflection coefficient (expressed as a fraction or percentage). Cloud type affects the albedo. Aircraft measurements show that the albedo of a complete overcast ranges from 44 to 50 per cent for cirrostratus to 90 per cent for cumulonimbus. Average albedo values, as determined by satellites, aircraft and surface measurements, are summarized in Table 3.2 (see Note 2).

The total (or global) solar radiation received at the surface on cloudy days is

$$S = S_0 [b + (1 - b)(1 - c)]$$

where S_0 = global solar radiation for clear skies;
c = cloudiness (fraction of sky covered);
b = a coefficient depending on cloud type and thickness; and the depth of atmosphere through which the radiation must pass.

For mean monthly values for the United States, $b \approx 0.35$, so that

$$S \approx S_0 [1 - 0.65c]$$

Table 3.2 The average (integrated) albedo of various surfaces (0.3–0.4 μm).

Planet earth	0.31
Global surface	0.14–0.16
Global cloud	0.23
Cumulonimbus	0.9
Stratocumulus	0.6
Cirrus	0.4–0.5
Fresh snow	0.8–0.9
Melting snow	0.4–0.6
Sand	0.30–0.35
Grass, cereal crops	0.18–0.25
Deciduous forest	0.15–0.18
Coniferous forest	0.09–0.15
Tropical rainforest	0.07–0.15
Water bodies*	0.06–0.10

Note: *Increases sharply at low solar angles.

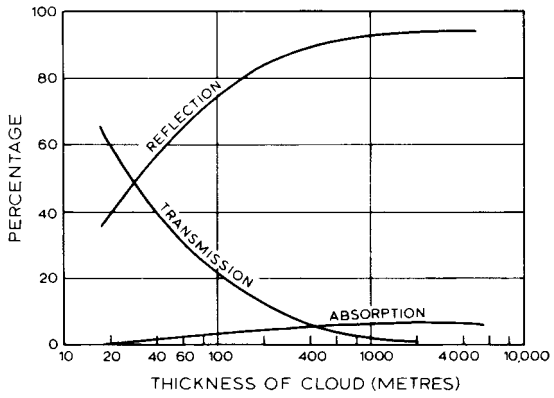

Figure 3.6 Percentage of reflection, absorption and transmission of solar radiation by cloud layers of different thickness.

Source: From Hewson and Longley (1944). Reprinted with permission. Copyright © CRC Press, Boca Raton, Florida.

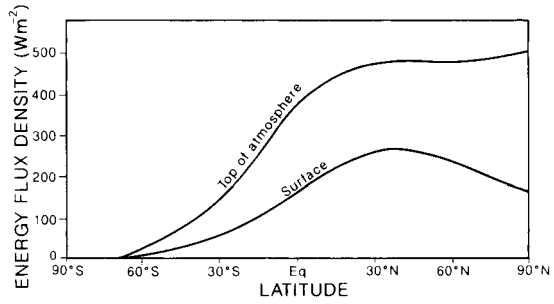

Figure 3.7 The average receipt of solar radiation with latitude at the top of the atmosphere and at the earth's surface during the June solstice.

The effect of cloud cover also operates in reverse, since it serves to retain much of the heat that would otherwise be lost from the earth by long-wave radiation throughout the day and night. In this way, cloud cover lessens appreciably the daily temperature range by preventing high maxima by day and low minima by night. As well as interfering with the transmission of radiation, clouds act as temporary thermal reservoirs because they absorb a certain proportion of the energy they intercept. The modest effects of cloud reflection and absorption of solar radiation are illustrated in Figures 3.5 to 3.7.

Global cloudiness is not yet known accurately. Ground-based observations are mostly at land stations and refer to a small (~ 250 km^2) area. Satellite estimates are derived from the reflected short-wave radiation and infra-red irradiance measurements, with various threshold assumptions for cloud presence/absence; typically they refer to a grid area of 2500 km^2 to 37,500 km^2. Surface-based observations tend to be about 10 per cent greater than satellite estimates due to the observer's perspective. Average winter and summer distributions of total cloud amount from surface observations are shown in Figure 3.8. The cloudiest areas are the Southern Ocean and the mid- to high-latitude North Pacific and North Atlantic storm tracks. Lowest amounts are over the Saharan–Arabian desert area (see Plate 1). Total global cloud cover is just over 60 per cent in January and July.

4 Effect of latitude

As Figure 3.4 has already shown, different parts of the earth's surface receive different amounts of solar radiation. The time of year is one factor controlling this, more radiation being received in summer than in winter because of the higher altitude of the sun and the longer days. Latitude is a very important control because this determines the duration of daylight and the distance travelled through the atmosphere by the oblique rays of the sun. However, actual calculations show the effect of the latter to be negligible near the poles, due apparently to the low vapour content of the air limiting tropospheric absorption. Figure 3.7 shows that in the upper atmosphere over the North Pole there is a marked maximum of solar radiation at the June solstice, yet only about 30 per cent is absorbed at the surface. This may be compared with the global average of 48 per cent of solar radiation being absorbed at the surface. The explanation lies in the high average cloudiness over the Arctic in summer and also in the high reflectivity of the snow and ice surfaces. This example illustrates the complexity of the radiation budget and the need to take into account the interaction of several factors.

A special feature of the latitudinal receipt of radiation is that the maximum temperatures experienced at the earth's surface do not occur at the equator, as one might expect, but at the tropics. A number of factors need to be taken into account. The apparent migration of the vertical sun is relatively rapid during its passage over the equator, but its rate slows down as it reaches the tropics. Between 6°N and 6°S the sun's rays remain almost vertically overhead for only thirty days during each of the spring and autumn equinoxes, allowing little time for any large buildup of surface heat and high temperatures. On the other hand, between 17.5° and 23.5° latitude the sun's rays shine down almost

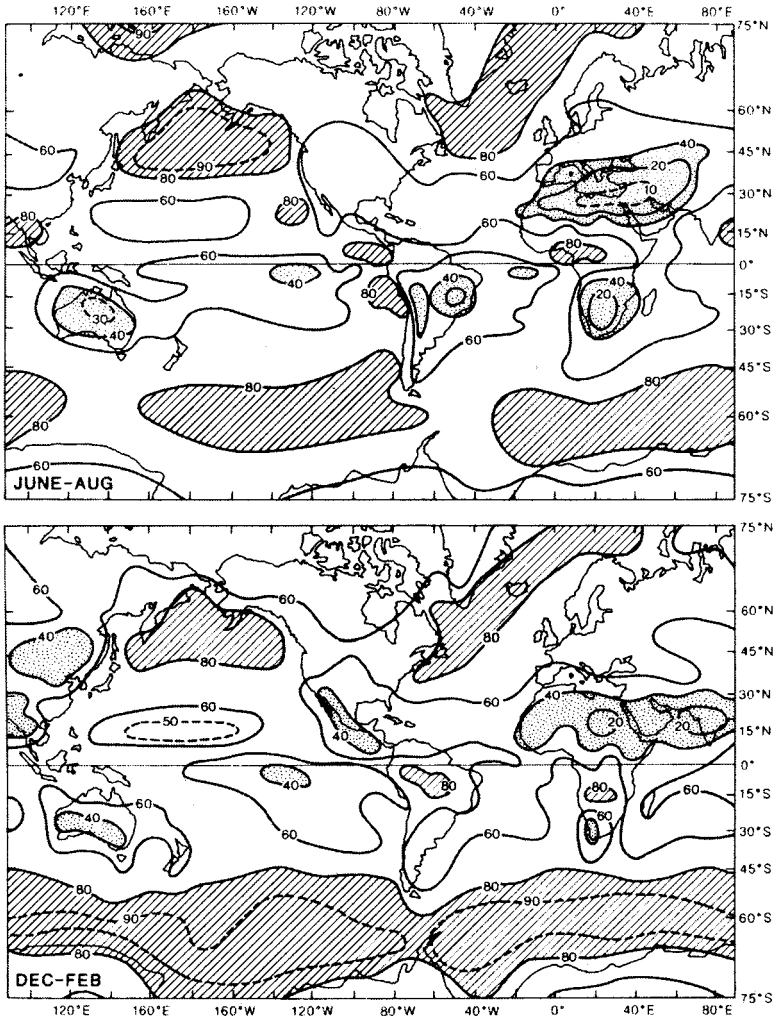

Figure 3.8 The global distribution of total cloud amount (per cent) derived from surface-based observations during the period 1971 to 1981, averaged for the months June to August (above) and December to February (below). High percentages are shaded and low percentages stippled.

Source: From London *et al.* (1989).

vertically for eighty-six consecutive days during the period of the solstice. This longer interval, combined with the fact that the tropics experience longer days than at the equator, makes the maximum zones of heating occur nearer the tropics than the equator. In the northern hemisphere, this poleward displacement of the zone of maximum heating is enhanced by the effect of *continentality* (see B.5, this chapter), while low cloudiness associated with the subtropical high-pressure belts is an additional factor. The clear skies allow large annual receipts of solar radiation in these areas. The net result of these influences is shown in Figure 3.9 in terms of the average annual solar radiation on a horizontal surface at ground level, and by Figure 3.10 in terms of the average daily maximum shade temperatures. Over land, the highest values occur at about 23°N and 10–15°S. Hence the mean annual *thermal equator* (i.e. the zone of maximum temperature) is located at about 5°N. Nevertheless, the mean air temperatures, reduced to mean sea-level, are related very broadly to latitude (see Figures 3.11A and B).

5 Effect of land and sea

Another important control on the effect of incoming solar radiation stems from the different ways in which land and sea are able to profit from it. Whereas water has a tendency to store the heat it receives, land, in contrast, quickly returns it to the atmosphere. There are several reasons for this.

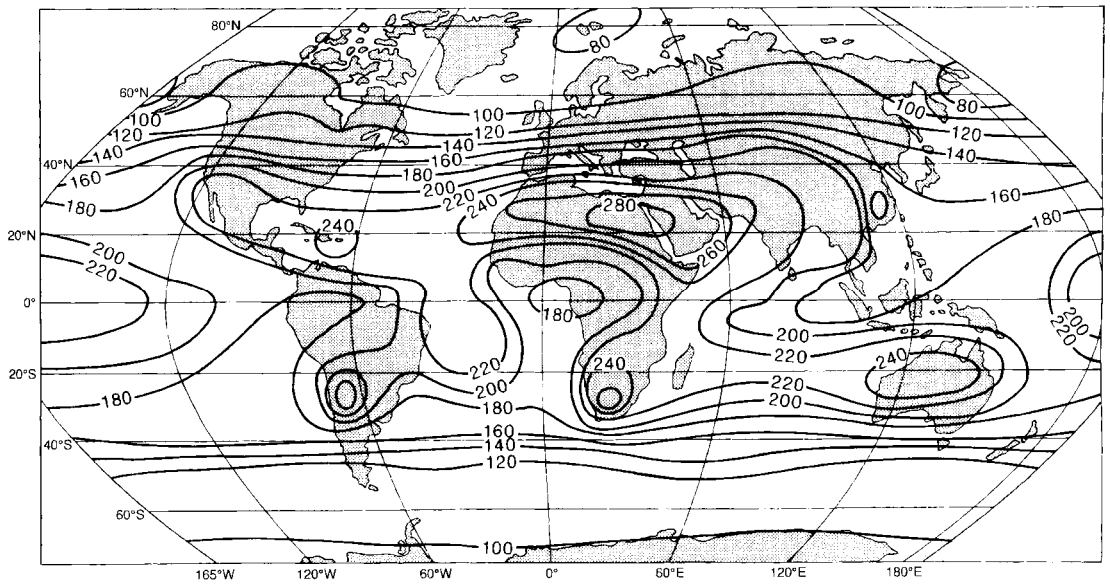

Figure 3.9 The mean annual global solar radiation ($Q + q$) (W m^{-2}) (i.e. on a horizontal surface at ground level). Maxima are found in the world's hot deserts, where as much as 80 per cent of the solar radiation annually incident on the top of the unusually cloud-free atmosphere reaches the ground.

Source: After Budyko *et al*. (1962).

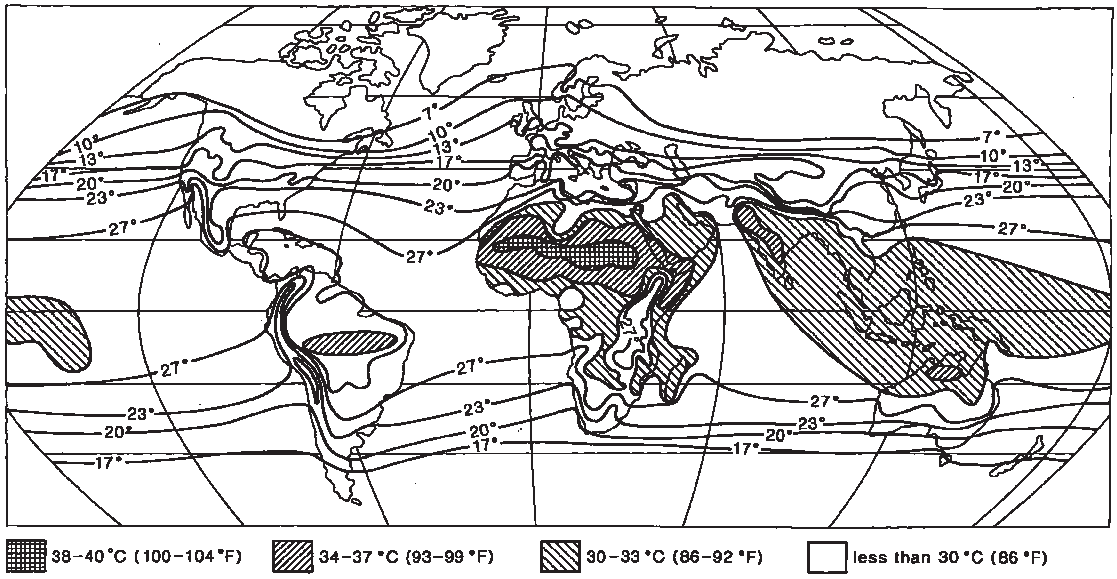

Figure 3.10 Mean daily maximum shade air temperature (C).

Source: After Ransom (1963).

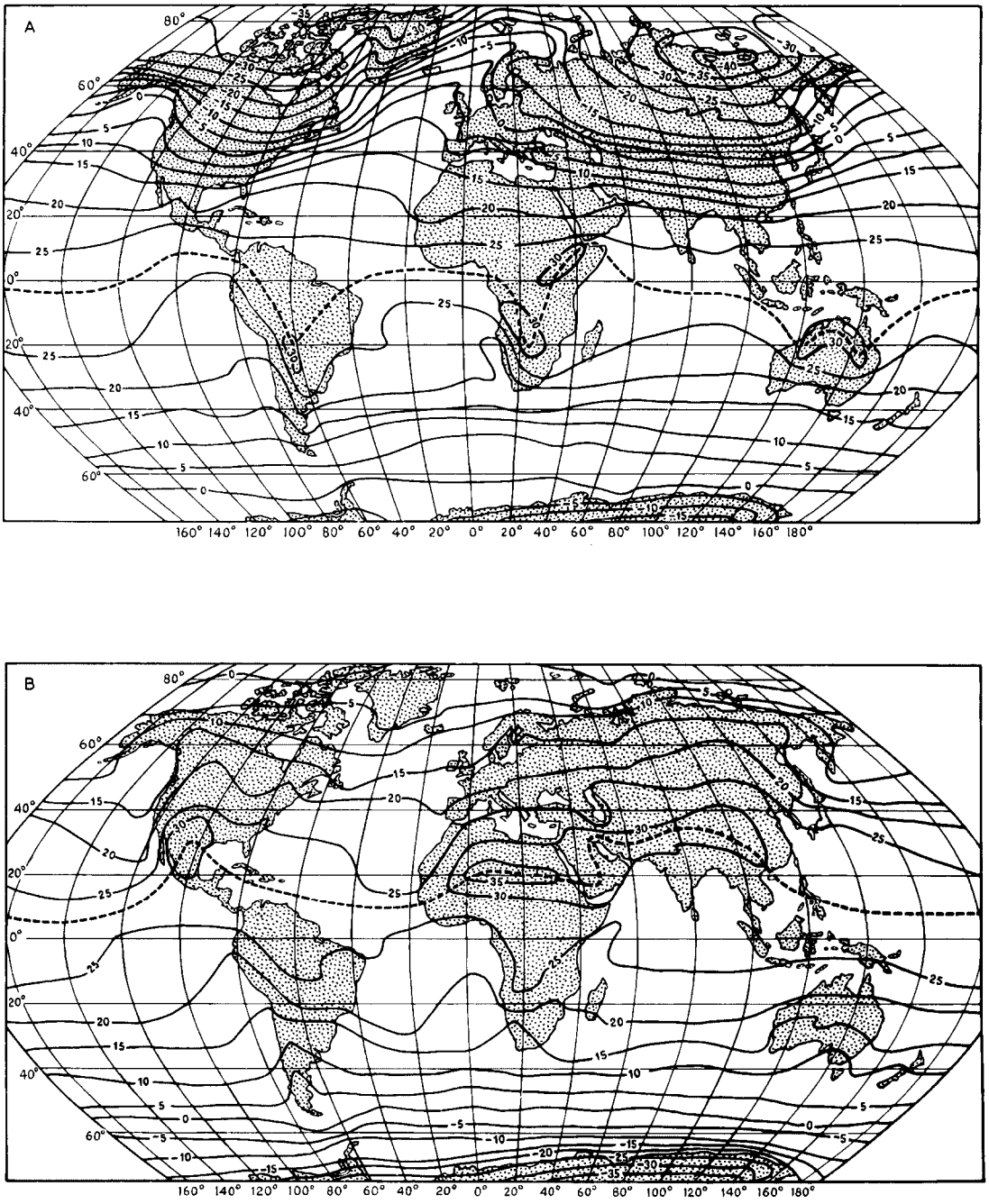

Figure 3.11 (A) Mean sea-level temperatures (°C) in January. The position of the thermal equator is shown approximately by the line dashes. (B) Mean sea-level temperatures (°C) in July. The position of the thermal equator is shown approximately by the line dashes.

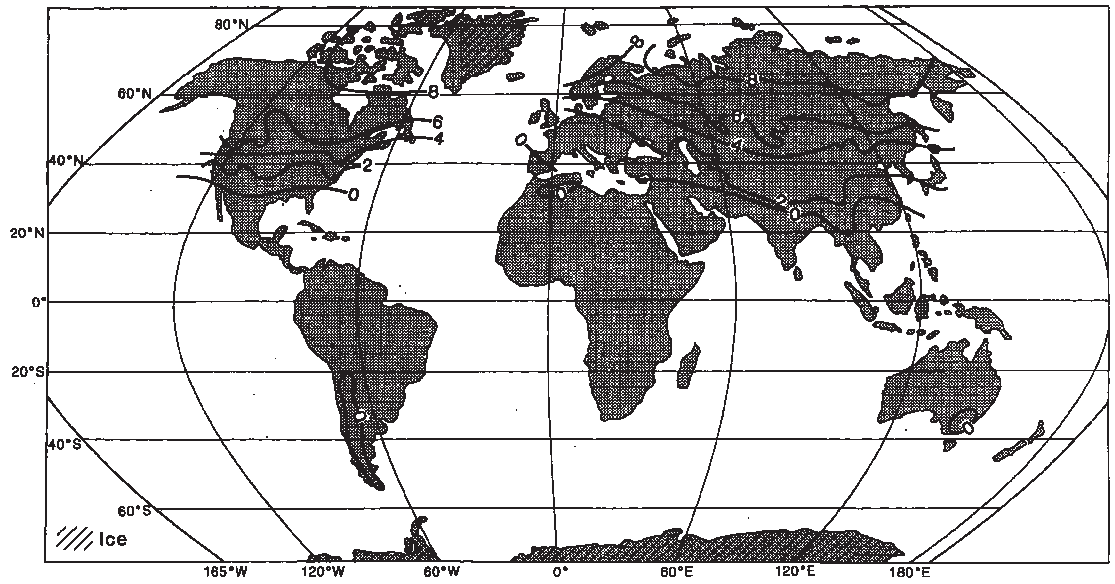

Figure 3.12 Average annual snow-cover duration (months).
Source: Henderson-Sellers and Wilson (1983).

A large proportion of the incoming solar radiation is reflected back into the atmosphere without heating the earth's surface. The proportion depends upon the type of surface (see Table 3.2). A sea surface reflects very little unless the angle of incidence of the sun's rays is large. The albedo for a calm water surface is only 2 to 3 per cent for a solar elevation angle exceeding 60°, but is more than 50 per cent when the angle is 15°. For land surfaces, the albedo is generally between 8 and 40 per cent of the incoming radiation. The figure for forests is about 9 to 18 per cent according to the type of tree and density of foliage (see Chapter 12C), for grass approximately 25 per cent, for cities 14 to 18 per cent, and for desert sand 30 per cent. Fresh snow may reflect as much as 90 per cent of solar radiation, but snow cover on vegetated, especially forested, surfaces is much less reflective (30 to 50 per cent). The long duration of snow cover on the northern continents (see Figure 3.12 and Plate A) causes much of the incoming radiation in winter to spring to be reflected. However, the global distribution of annual average surface albedo (Figure 3.13A) shows mainly the influence of the snow-covered Arctic sea ice and Antarctic ice sheet (compare Figure 3.13B for planetary albedo).

The global solar radiation absorbed at the surface is determined from measurements of radiation incident on the surface and its albedo (a). It may be expressed as

$$S(100 - a)$$

where the albedo is a percentage. A snow cover will absorb only about 15 per cent of the incident radiation, whereas for the sea the figure generally exceeds 90 per cent. The ability of the sea to absorb the heat received also depends upon its transparency. As much as 20 per cent of the radiation penetrates as far down as 9 m (30 ft). Figure 3.14 illustrates how much energy is absorbed by the sea at different depths. However, the heat absorbed by the sea is carried down to considerable depths by the turbulent mixing of water masses by the action of waves and currents. Figure 3.15, for example, illustrates the mean monthly variations with depth in the upper 100 metres of the waters of the eastern North Pacific (around 50°N, 145°W); it shows the development of the seasonal thermocline under the influences of surface heating, vertical mixing and surface conduction.

A measure of the difference between the subsurfaces of land and sea is given in Figure 3.16, which shows ground temperatures at Kaliningrad (Königsberg) and sea temperature deviations from the annual mean at various depths in the Bay of Biscay. Heat transmission in the soil is carried out almost wholly by conduction, and the degree of conductivity varies with the moisture content and porosity of each particular soil.

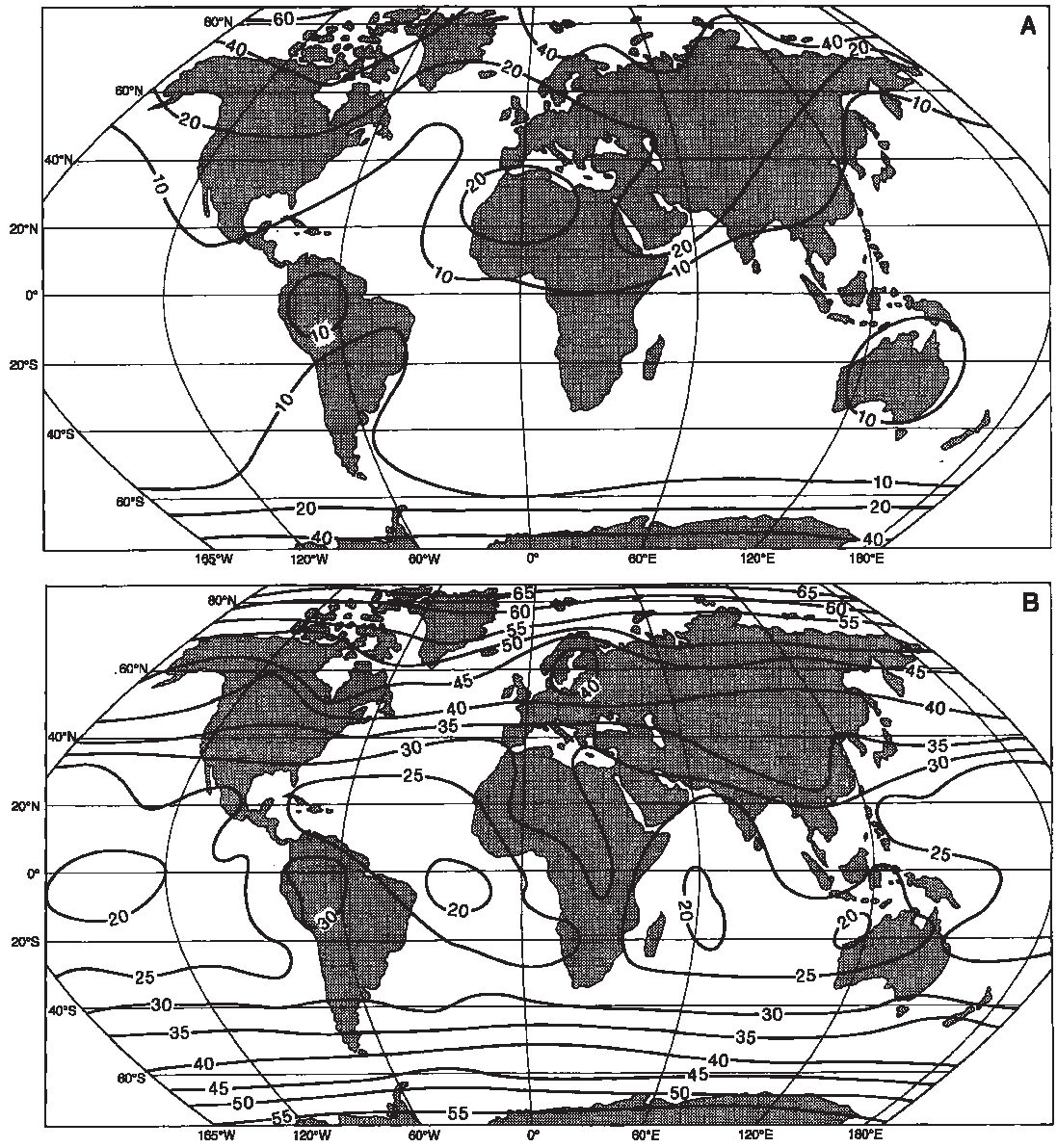

Figure 3.13 Mean annual albedos (per cent): (A) At the earth's surface. (B) On a horizontal surface at the top of the atmosphere.

Source: After Hummel and Reck; from Henderson-Sellers and Wilson (1983), and Stephens *et al*. (1981), by permission of the American Geophysical Union.

Air is an extremely poor conductor, and for this reason a loose, sandy soil surface heats up rapidly by day, as the heat is not conducted away. Increased soil moisture tends to raise the conductivity by filling the soil pores, but too much moisture increases the soil's heat capacity, thereby reducing the temperature response. The relative depths over which the annual and diurnal temperature variations are effective in wet and dry soils are approximately as follows:

	Diurnal variation	*Annual variation*
Wet soil	0.5 m	9 m
Dry sand	0.2 m	3 m

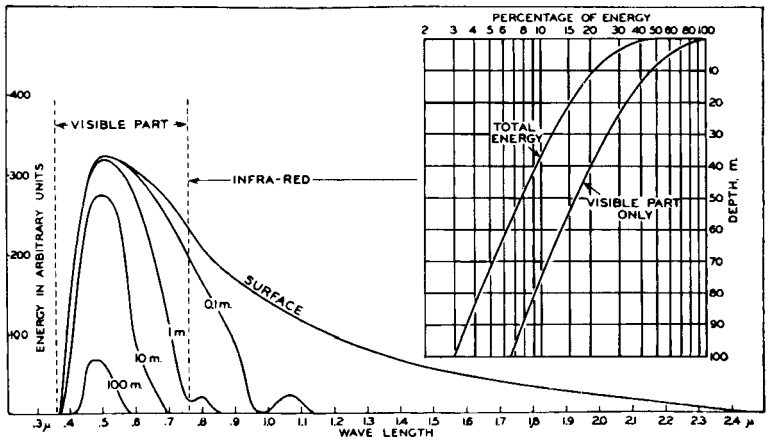

Figure 3.14 Schematic representation of the energy spectrum of the sun's radiation (in arbitrary units) that penetrates the sea surface to depths of 0.1, 1, 10 and 100 m. This illustrates the absorption of infra-red radiation by water, and also shows the depths to which visible (light) radiation penetrates.

Source: From Sverdrup (1945).

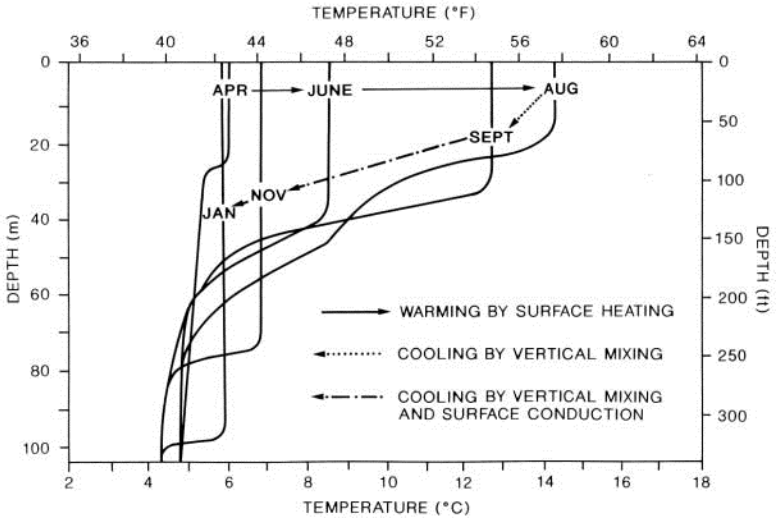

Figure 3.15 Mean monthly variations of temperature with depth in the surface waters of the eastern North Pacific. The layer of rapid temperature change is termed the thermocline.

Source: After Tully and Giovando (1963). Reproduced by permission of the Royal Society of Canada.

However, the *actual* temperature change is greater in dry soils. For example, the following values of diurnal temperature range have been observed during clear summer days at Sapporo, Japan:

	Sand	*Loam*	*Peat*	*Clay*
Surface	40°C	33°C	23°C	21°C
5 cm	20	19	14	14
15 cm	7	6	2	4

The different heating qualities of land and water are also accounted for partly by their different *specific heats*. The specific heat (c) of a substance can be represented by the number of thermal units required to raise a unit mass of it through 1°C (4184 J kg^{-1} K^{-1}). The specific heat of water is much greater than for most other common substances, and water must absorb five times as much heat energy to raise its temperature by the same amount as a comparable mass of dry soil. Thus for dry sand, $c = 840$ J kg^{-1} K^{-1}.

If unit volumes of water and soil are considered, the heat capacity, ρc, of the water, where ρ = density ($\rho c = 4.18 \times 10^6$ J m^{-3} K^{-1}), exceeds that of the sand approximately threefold ($\rho c = 1.3 \times 1.6$ J m^{-3} K^{-1}) if the sand is dry and twofold if it is wet. When this water is cooled the situation is reversed, for then a large quantity of heat is released. A metre-thick layer of sea water being cooled by as little as 0.1°C will release enough heat to

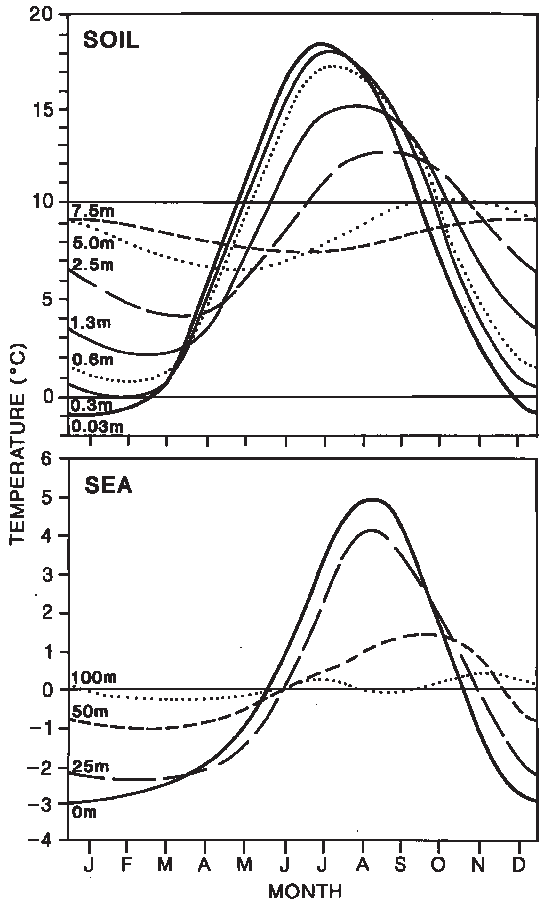

Figure 3.16 Annual variation of temperature at different depths in soil at Kaliningrad, European Russia (above) and in the water of the Bay of Biscay (at approximately 47° N, 12°W) (below), illustrating the relatively deep penetration of solar energy into the oceans as distinct from that into land surfaces. The bottom figure shows the temperature deviations from the annual mean for each depth.

Sources: Geiger (1965) and Sverdrup (1945).

raise the temperature of an approximately 30 m thick air layer by 10°C. In this way, the oceans act as a very effective reservoir for much of the world's heat. Similarly, evaporation of sea water causes large heat expenditure because a great amount of energy is needed to evaporate even a small quantity of water (see Chapter 3C).

The thermal role of the ocean is an important and complex one (see Chapter 7D). The ocean comprises three thermal layers:

1 A seasonal boundary, or upper mixed layer, lying above the thermocline. This is less than 100 m deep in the tropics but is hundreds of metres deep in the subpolar seas. It is subject to annual thermal mixing from the surface (see Figure 3.15).
2 A warm water sphere or lower mixed layer. This underlies layer 1 and slowly exchanges heat with it down to many hundreds of metres.
3 The deep ocean. This contains some 80 per cent of the total oceanic water volume and exchanges heat with layer 1 in the polar seas.

This vertical thermal circulation allows global heat to be conserved in the oceans, thus damping down the global effects of climatic change produced by thermal forcing (see Chapter 13B). The time for heat energy to diffuse within the upper mixed layer is two to seven months, within the lower mixed layer seven years, and within the deep ocean upwards of 300 years. The comparative figure for the outer thermal layer of the solid earth is only eleven days.

These differences between land and sea help to produce what is termed *continentality*. Continentality implies, first, that a land surface heats and cools much more quickly than that of an ocean. Over the land, the lag between maximum (minimum) periods of radiation and the maximum (minimum) surface temperature is only one month, but over the ocean and at coastal stations the lag is up to two months. Second, the annual and diurnal ranges of temperature are greater in continental than in coastal locations. Figure 3.17 illustrates the annual variation of temperature at Toronto, Canada and Valentia, western Ireland, while diurnal temperature ranges experienced in continental and maritime areas are described below (see pp. 55–6). The third effect of continentality results from the global distribution of the landmasses. The smaller ocean area of the northern hemisphere causes the boreal summer to be warmer but its are winters colder on average than the austral equivalents of the southern hemisphere (summer, 22.4°C versus 17.1°C; winter, 8.1°C versus 9.7°C). Heat storage in the oceans causes them to be warmer in winter and cooler in summer than land in the same latitude, although ocean currents give rise to some local departures from this rule. The distribution of temperature anomalies for the latitude in January and July (Figure 3.18) illustrates the significance of continentality and the influence of the warm currents in the North Atlantic and the North Pacific in winter.

Sea-surface temperatures can now be estimated by the use of infra-red satellite imagery (see C, this

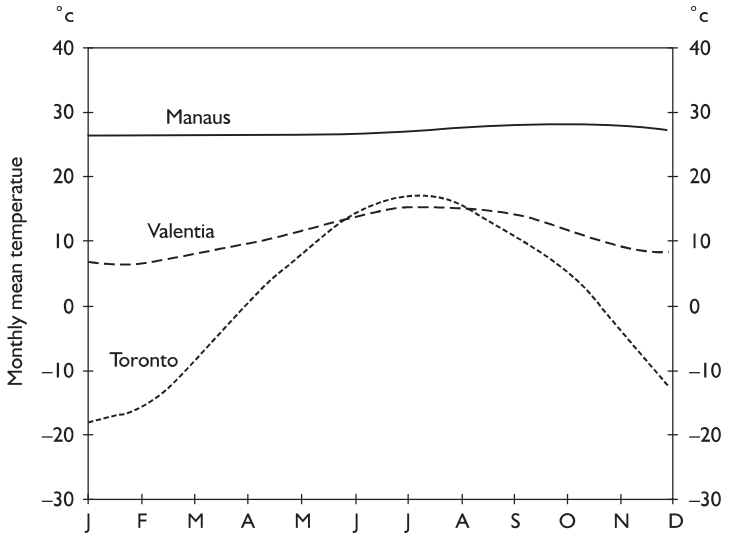

Figure 3.17 Mean annual temperature regimes in various climates. Manaus, Brazil (equatorial), Valentia, Ireland (temperate maritime) and Toronto, Canada (temperate continental).

chapter). Plate B shows a false-colour satellite thermal image of the western North Atlantic showing the relatively warm, meandering Gulf Stream. Maps of sea-surface temperatures are now routinely constructed from such images.

6 Effect of elevation and aspect

When we come down to the local scale, differences in the elevation of the land and its *aspect* (that is, the direction that the surface faces) strongly control the amount of solar radiation received.

High elevations that have a much smaller mass of air above them (see Figure 2.13) receive considerably more direct solar radiation under clear skies than do locations near sea-level due to the concentration of water vapour in the lower troposphere (Figure 3.19). On average in middle latitudes the intensity of incident solar radiation increases by 5 to 15 per cent for each 1000 m increase in elevation in the lower troposphere. The difference between sites at 200 and 3000 m in the Alps, for instance, can amount to 70 W m^{-2} on cloudless summer days. However, there is also a correspondingly greater net loss of terrestrial radiation at higher elevations because the low density of the overlying air results in a smaller fraction of the outgoing radiation being absorbed. The overall effect is invariably complicated by the greater cloudiness associated with most mountain ranges, and it is therefore impossible to generalize from the limited data available.

Figure 3.20 illustrates the effect of aspect and slope angle on theoretical maximum solar radiation receipts at two locations in the northern hemisphere. The general effect of latitude on insolation amounts is clearly shown, but it is also apparent that increasing latitude causes a relatively greater radiation loss for north-facing slopes, as distinct from south-facing ones. The radiation intensity on a sloping surface (I_s) is

$$I_s = I_o \cos i$$

where i = the angle between the solar beam and a beam normal to the sloping surface. Relief may also affect the quantity of insolation and the duration of direct sunlight when a mountain barrier screens the sun from valley floors and sides at certain times of day. In many Alpine valleys, settlement and cultivation are noticeably concentrated on southward-facing slopes (the adret or sunny side), whereas northward slopes (ubac or shaded side) remain forested.

7 Variation of free-air temperature with height

Chapter 2C described the gross characteristics of the vertical temperature profile in the atmosphere. We will now examine the vertical temperature gradient in the lower troposphere.

Vertical temperature gradients are determined in part by energy transfers and in part by vertical motion of the

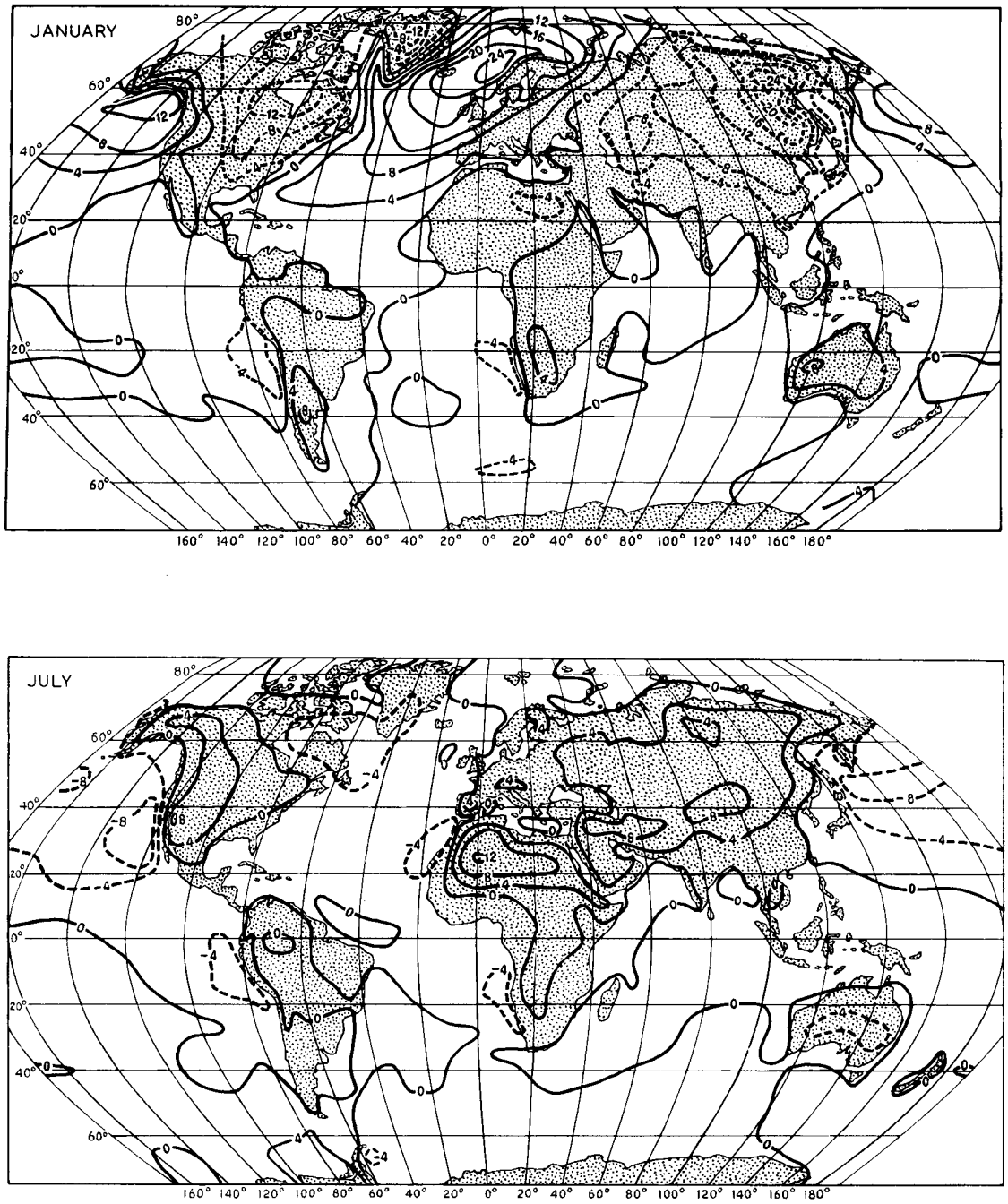

Figure 3.18 World temperature anomalies (i.e. the difference between recorded temperatures °C and the mean for that latitude) for January and July. Solid lines indicate positive, and dashed lines negative, anomalies.

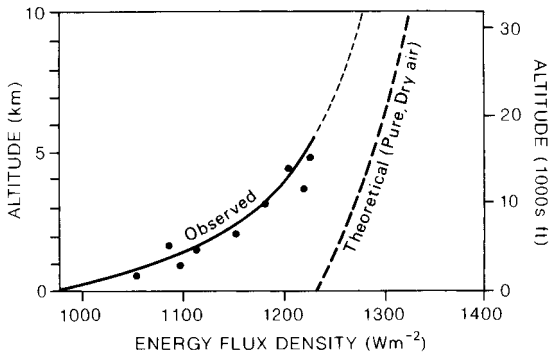

Figure 3.19 Direct solar radiation as a function of altitude observed in the European Alps. The absorbing effects of water vapour and dust, particularly below about 3000 m, are shown by comparison with a theoretical curve for an ideal atmosphere.

Source: After Albetti, Kastrov, Kimball and Pope; from Barry (1992).

air. The various factors interact in a highly complex manner. The energy terms are the release of latent heat by condensation, radiative cooling of the air and sensible heat transfer from the ground. Horizontal temperature advection, by the motion of cold and warm airmasses, may also be important. Vertical motion is dependent on the type of pressure system. High-pressure areas are generally associated with descent and warming of deep layers of air, hence decreasing the temperature gradient and frequently causing temperature inversions in the lower troposphere. In contrast, low-pressure systems are associated with rising air, which cools upon expansion and increases the vertical temperature gradient. Moisture is an additional complicating factor (see Chapter 3E), but it remains true that the middle and upper troposphere is relatively cold above a surface low-pressure area, leading to a steeper temperature gradient.

The overall vertical decrease of temperature, or *lapse rate*, in the troposphere is about 6.5°C/km. However, this is by no means constant with height, season or location. Average global values calculated by C. E. P. Brooks for July show increasing lapse rate with height: about 5°C/km in the lowest 2 km, 6°C/km between 4 and 5km, and 7°C/km between 6 and 8 km. The seasonal regime is very pronounced in continental regions with cold winters. Winter lapse rates are generally small and, in areas such as central Canada or eastern Siberia, may even be negative (i.e. temperatures increase with height in the lowest layer) as a result of excessive radiational

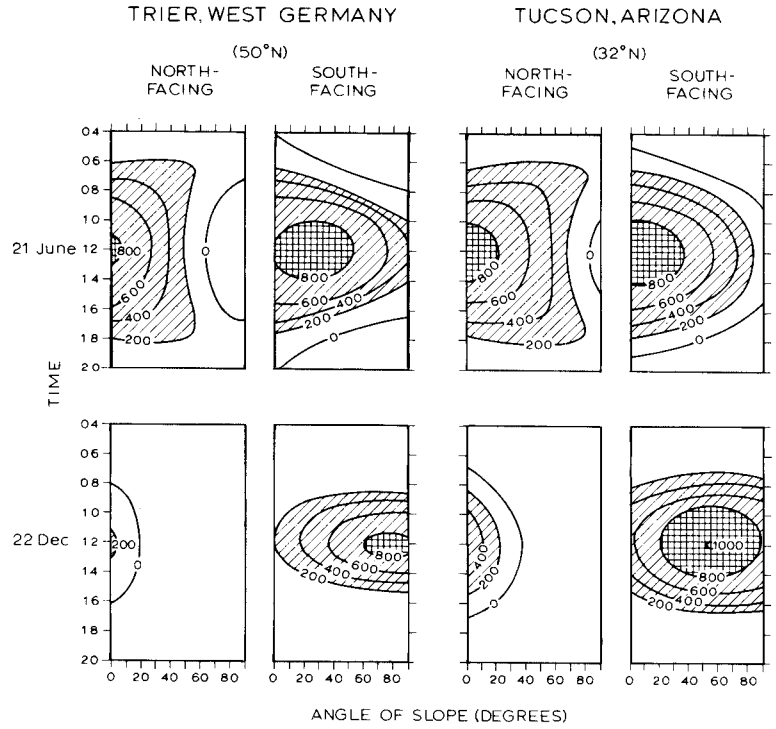

Figure 3.20 Average direct beam solar radiation (W m^{-2}) incident at the surface under cloudless skies at Trier, West Germany, and Tucson, Arizona, as a function of slope, aspect, time of day and season of year.

Source: After Geiger (1965) and Sellers (1965).

cooling over a snow surface. A similar situation occurs when dense, cold air accumulates in mountain basins on calm, clear nights. On such occasions, mountain summits may be many degrees warmer than the valley floor below (see Chapter 6C.2). For this reason, the adjustment of average temperature of upland stations to mean sea-level may produce misleading results. Observations in Colorado at Pike's Peak (4301 m) and Colorado Springs (1859 m) show the mean lapse rate to be 4.1°C/km in winter and 6.2°C/km in summer. It should be noted that such topographic lapse rates may bear little relation to free air lapse rates in nocturnal radiation conditions, and the two must be carefully distinguished.

In the Arctic and over Antarctica, surface temperature inversions persist for much of the year. In winter the Arctic inversion is due to intense radiational cooling, but in summer it is the result of the surface cooling of advected warmer air. The tropical and subtropical deserts have very steep lapse rates in summer causing considerable heat transfer from the surface and generally ascending motion; subsidence associated with high-pressure cells is predominant in the desert zones in winter. Over the subtropical oceans, sinking air leads to warming and a subsidence inversion near the surface (see Chapter 13).

C TERRESTRIAL INFRA-RED RADIATION AND THE GREENHOUSE EFFECT

Radiation from the sun is predominantly short-wave, whereas that leaving the earth is long-wave, or infra-red, radiation (see Figure 3.1). The infra-red emission from the surface is slightly less than that from a black body at the same temperature and, accordingly, Stefan's Law (see p. 33) is modified by an emissivity coefficient (ε), which is generally between 0.90 and 0.95, i.e. $F = \varepsilon\sigma T^4$. Figure 3.1 shows that the atmosphere is highly absorbent to infra-red radiation (due to the effects of water vapour, carbon dioxide and other trace gases), except between about 8.5 and 13.0 μm – the 'atmospheric window'. The opaqueness of the atmosphere to infra-red radiation, relative to its transparency to short-wave radiation, is commonly referred to as the *greenhouse effect*. However, in the case of an actual greenhouse, the effect of the glass roof is probably as significant in reducing cooling by restricting the turbulent heat loss as it is in retaining the infra-red radiation.

The total 'greenhouse' effect results from the net infra-red absorption capacity of water vapour, carbon dioxide and other trace gases – methane (CH_4), nitrous oxide (N_2O) and tropospheric ozone (O_3). These gases absorb strongly at wavelengths within the atmospheric window region, in addition to their other absorbing bands (see Figure 3.1 and Table 3.3). Moreover, because concentrations of these trace gases are low, their radiative effects increase approximately linearly with concentration, whereas the effect of CO_2 is related to the logarithm of the concentration. In addition, because of the long atmospheric residence time of nitrous oxide (132 years) and CFCs (65 to 140 years), the cumulative effects of human activities will be substantial. It is estimated that between 1765 and 2000, the radiative effect of increased CO_2 concentration was 1.5 W m^{-2}, and of all trace gases about 2.5 W m^{-2} (cf. the solar constant value of 1366 W m^{-2}).

The net warming contribution of the natural (non-anthropogenic) greenhouse gases to the mean 'effective' planetary temperature of 255 K (corresponding to the emitted infra-red radiation) is approximately 33 K. Water vapour accounts for 21 K of this amount, carbon dioxide 7 K, ozone 2 K, and other trace gases (nitrous oxide, methane) about 3 K. The present global mean surface temperature is 288 K, but the surface was considerably warmer during the early evolution of the earth, when the atmosphere contained large quantities of methane, water vapour and ammonia. The largely carbon dioxide atmosphere of Venus creates a 500 K greenhouse effect on that planet.

Stratospheric ozone absorbs significant amounts of both incoming ultraviolet radiation, harmful to life, and outgoing terrestrial long-wave re-radiation, so that its overall thermal role is a complex one. Its net effect on earth surface temperatures depends on the elevation at which the absorption occurs, being to some extent a trade-off between short- and long-wave absorption in that:

1 An increase of ozone above about 30 km absorbs relatively more incoming short-wave radiation, causing a net *decrease* of surface temperatures.
2 An increase of ozone below about 25 km absorbs relatively more outgoing long-wave radiation, causing a net *increase* of surface temperatures.

Long-wave radiation is not merely terrestrial in the narrow sense. The atmosphere radiates to space, and

Table 3.3 Influence of greenhouse gases on atmospheric temperature.

Gas	*Centres of main absorption bands (μm)*	*Temperature increase (K) for ×2 present concentration*	*Global warming potential on a weight basis (kg^{-1} of air)†*
Water vapour (H_2O)	6.3–8.0, >15 (8.3–12.5)*		
Carbon dioxide (CO_2)	(5.2), (10), 14.7	3.0 ± 1.5	1
Methane (CH_4)	6.52, 7.66	0.3–0.4	11
Ozone (O_3)	4.7, 9.6, (14.3)	0.9	
Nitrous oxide (N_2O)	7.78, 8.56, 17.0	0.3	270
Chlorofluoromethanes			
($CFCl_3$)	4.66, 9.22, 11.82 6	0.1	3400
(CF_2Cl_2)	8.68, 9.13, 10.93		7100

Notes: * Important in moist atmospheres.
† Refers to direct annual radiative forcing for the surface-troposphere system.

Sources: After Campbell; Ramanathan; Lashof and Ahuja; Luther and Ellingson; IPCC (1992).

THE GREENHOUSE EFFECT

box 3.1 topical issue

The *natural* greenhouse effect of the earth's atmosphere is attributable primarily to water vapour. It accounts for 21 K of the 33 K difference between the effective temperature of a dry atmosphere and the real atmosphere through the trapping of infra-red radiation. Water vapour is strongly absorptive around 2.4–3.1 μm, 4.5–6.5 μm and above 16 μm. The concept of greenhouse gas-induced warming is commonly applied to the effects of the increases in atmospheric carbon dioxide concentrations resulting from *anthropogenic* activities, principally the burning of fossil fuels. Sverre Arrhenius in Sweden drew attention to this possibility in 1896, but observational evidence was forthcoming only some forty years later (Callendar, 1938, 1959). However, a careful record of of atmospheric concentrations of carbon dioxide was lacking until Charles Keeling installed calibrated instruments at the Mauna Loa Observatory, Hawaii, in 1957. Within a decade, these observations became the global benchmark . They showed an annual cycle of about 5 ppm at the Observatory, caused by the biospheric uptake and release, and the *c*. 0.5 per cent annual increase in CO_2, from 315 ppm in 1957 to 370 ppm in 2001, due to fossil fuel burning. The annual increase is about half of the total emission due to CO_2 uptake by the oceans and the land biosphere. The principal absorption band for radiation by carbon dioxide is around 14–16 μm, but there are others at 2.6 and 4.2 μm. Most of the effect of increasing CO_2 concentration is by enhanced absorption in the latter, as the main band is almost saturated. The sensitivity of mean global air temperature to a doubling of CO_2 in the range 2 to 5°C, while a removal of all atmospheric CO_2 might lower the mean surface temperature by more than 10°C.

The important role of other trace greenhouse gases (methane and fluorocarbons) recognized in the 1980s and many additional trace gases began to be monitored and their past histories reconstructed from ice core records. These show that the pre-industrial level of CO_2 was 280 ppm and methane 750 ppb; these values decreased to about 180 ppm and 350 ppb, respectively, during the maximum phases of continental glaciation in the Ice Age.

The positive feedback effect of CO_2, which involves greenhouse gas-induced warming leading to an enhanced hydrological cycle with a larger atmospheric vapour content and therefore further warming, is still not well resolved quantitatively.

clouds are particularly effective since they act as black bodies. For this reason, cloudiness and cloud-top temperature can be mapped from satellites by day and by night using infra-red sensors (see Plates 2, 3 and 15, where high clouds appear cold). Radiative cooling of cloud layers averages about 1.5°C per day.

For the globe as a whole, satellite measurements show that in cloud-free conditions the mean absorbed solar radiation is approximately 285W m^{-2}, whereas the emitted terrestrial radiation is 265W m^{-2}. Including cloud-covered areas, the corresponding global values are 235 W m^{-2} for both terms. Clouds reduce the absorbed solar radiation by 50 W m^{-2}, but reduce the emitted radiation by only 30 W m^{-2}. Hence global cloud cover causes a net radiative loss of about 20 W m^{-2}, due to the dominance of cloud albedo reducing short-wave radiation absorption. In lower latitudes this effect is much larger (up to –50 to –100 W m^{-2}), whereas in high latitudes the two factors are close to balance, or the increased infra-red absorption by clouds may lead to a small positive value. These results are important in terms of changing concentrations of greenhouse gases, since the net radiative forcing by cloud cover is four times that expected from CO_2 doubling (see Chapter 13).

D HEAT BUDGET OF THE EARTH

We can now summarize the net effect of the transfers of energy in the earth–atmosphere system averaged over the globe and over an annual period.

The incident solar radiation averaged over the globe is

$$\text{Solar constant} \times \pi r^2 / 4\pi r^2$$

where r = radius of the earth and $4\pi r^2$ is the surface area of a sphere. This figure is approximately 342 W m^{-2}, or 11×10^9 J m^{-2} yr^{-1} (10^9 J = 1GJ); for convenience we will regard it as 100 units. Referring to Figure 3.21, incoming radiation is absorbed in the stratosphere (3 units), by ozone mainly, and 20 units are absorbed in the troposphere by carbon dioxide (1), water vapour (13), dust (3) and water droplets in clouds (3). Twenty units are reflected back to space from clouds, which

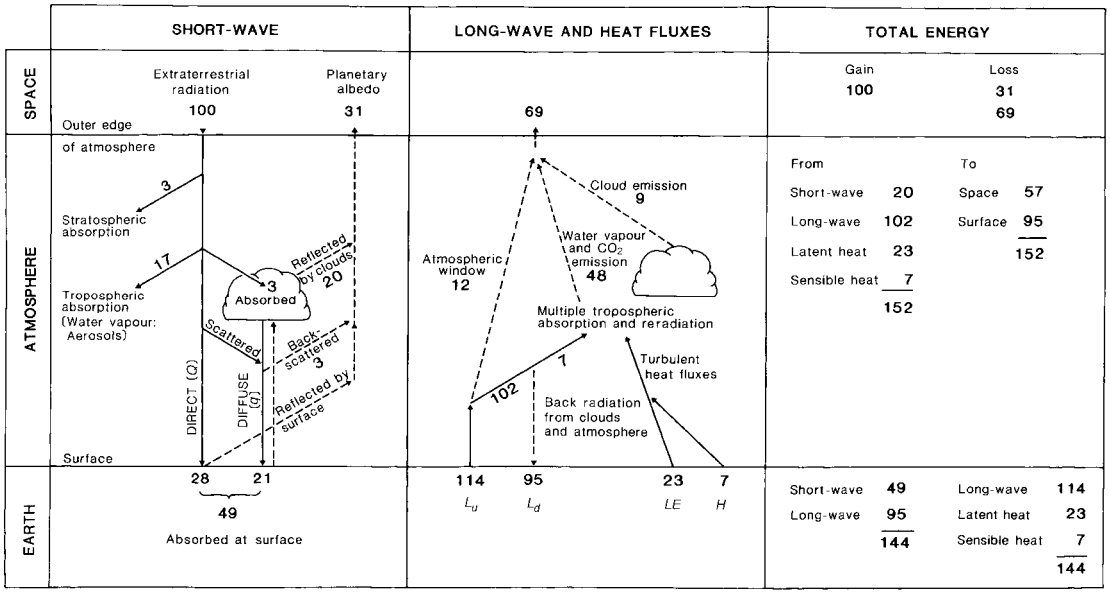

Figure 3.21 The balance of the atmospheric energy budget. The transfers are explained in the text. Solid lines indicate energy gains by the atmosphere and surface in the left-hand diagram and the troposphere in the right-hand diagram. The exchanges are referred to 100 units of incoming solar radiation at the top of the atmosphere (equal to 342 W m^{-2}).

Source: After Kiehl and Trenberth (1997) From *Bulletin of the American Meteorological Society*, by permission of the American Meteorological Society.

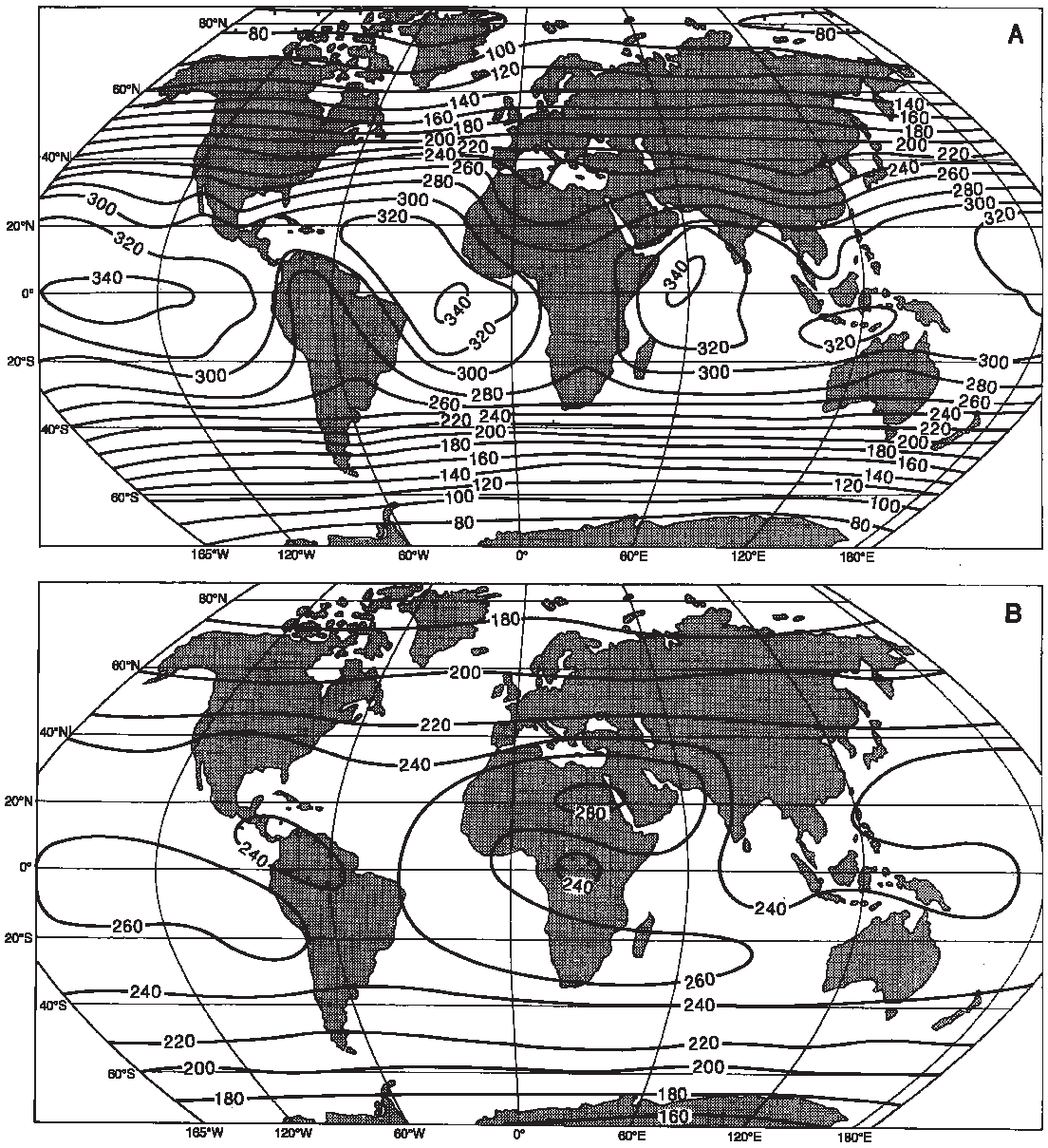

Figure 3.22 Planetary short- and long-wave radiation (Wm^{-2}). (A) Mean annual absorbed short-wave radiation for the period April 1979 to March 1987. (B) Mean annual net planetary long-wave radiation (L_n) on a horizontal surface at the top of the atmosphere.

Sources: (A) Ardanuy *et al*. (1992) and Kyle *et al*. (1993) *From Bulletin of the American Meteorological Society*, by permission of the American Meteorological Society. (B) Stephens *et al*. (1981).

cover about 62 per cent of the earth's surface on average. A further nine units are similarly reflected from the surface and three units are returned by atmospheric scattering. The total reflected radiation is the *planetary albedo* (31 per cent or 0.31). The remaining forty-nine units reach the earth either directly ($Q = 28$) or as diffuse radiation ($q = 21$) transmitted via clouds or by downward scattering.

The pattern of outgoing terrestrial radiation is quite different (see Figure 3.22). The black-body radiation,

assuming a mean surface temperature of 288 K, is equivalent to 114 units of infra-red (long-wave) radiation. This is possible since most of the outgoing radiation is reabsorbed by the atmosphere; the *net* loss of infra-red radiation at the surface is only nineteen units. These exchanges represent a time-averaged state for the whole globe. Recall that solar radiation affects only the sunlit hemisphere, where the incoming radiation exceeds 342 W m^{-2}. Conversely, no solar radiation is received by the night-time hemisphere. Infra-red exchanges continue, however, due to the accumulated heat in the ground. Only about twelve units escape through the atmospheric window directly from the surface. The atmosphere itself radiates fifty-seven units to space (forty-eight from the emission by atmospheric water vapour and CO_2 and nine from cloud emission), giving a total of sixty-nine units (L_u); the atmosphere in turn radiates ninety-five units back to the surface (L_d); thus $L_u + L_d = L_n$ is negative.

These radiation transfers can be expressed symbolically:

$$R_n = (Q + q)\,(1 - a) + L_n$$

where R_n = net radiation, $(Q + q)$ = global solar radiation, a = albedo and L_n = net long-wave radiation. At the surface, R_n = 30 units. This surplus is conveyed to the atmosphere by the turbulent transfer of sensible heat, or enthalpy (seven units), and latent heat (twenty-three units):

$$R_n = LE + H$$

where H = sensible heat transfer and LE = latent heat transfer. There is also a flux of heat into the ground (B.5, this chapter), but for annual averages this is approximately zero.

Figure 3.22 summarizes the total balances at the surface (± 144 units) and for the atmosphere (± 152 units). The total absorbed solar radiation and emitted radiation for the entire earth–atmosphere system is estimated to be ±7 GJ m^{-2} yr^{-1} (± 69 units). Various uncertainties are still to be resolved in these estimates. The surface short-wave and long-wave radiation budgets have an uncertainty of about 20 W m^{-2}, and the turbulent heat fluxes of about 10 W m^{-2}.

Satellite measurements now provide global views of the energy balance at the top of the atmosphere. The incident solar radiation is almost symmetrical about the equator in the annual mean (cf. Table 3.1). The mean annual totals on a horizontal surface at the top of the atmosphere are approximately 420 W m^{-2} at the equator and 180 W m^{-2} at the poles. The distribution of the planetary albedo (see Figure 3.13B) shows the lowest values over the low-latitude oceans compared with the more persistent areas of cloud cover over the continents. The highest values are over the polar ice-caps. The resulting planetary short-wave radiation ranges from 340 Wm^{-2} at the equator to 80 Wm^{-2} at the poles. The net (outgoing) long-wave radiation (Figure 3.22B) shows the smallest losses where the temperatures are lowest and highest losses over the largely clear skies of the Saharan desert surface and over low-latitude oceans. The difference between Figure 3.22A and 3.22B represents the net radiation of the earth–atmosphere system which achieves balance about latitude 30°. The consequences of a low-latitude energy surplus and a high-latitude deficit are examined below.

The diurnal and annual variations of temperature are related directly to the local energy budget. Under clear skies, in middle and lower latitudes, the diurnal regime of radiative exchanges generally shows a midday maximum of absorbed solar radiation (see Figure 3.23A). A maximum of infra-red (long-wave) radiation (see Figure 3.1) is also emitted by the heated ground surface at midday, when it is warmest. The atmosphere re-radiates infra-red radiation downward, but there is a net loss at the surface (L_n). The difference between the absorbed solar radiation and L_n is the net radiation, R_n; this is generally positive between about an hour after sunrise and an hour or so before sunset, with a midday maximum. The delay in the occurrence of the maximum air temperature until about 14:00 hours local time (Figure 3.23B) is caused by the gradual heating of the air by convective transfer from the ground. Minimum R_n occurs in the early evening, when the ground is still warm; there is a slight increase thereafter. The temperature decrease after midday is slowed by heat supplied from the ground. Minimum air temperature occurs shortly after sunrise due to the lag in the transfer of heat from the surface to the air. The annual pattern of the net radiation budget and temperature regime is closely analogous to the diurnal one, with a seasonal lag in the temperature curve relative to the radiation cycle, as noted above (p. 47).

There are marked latitudinal variations in the diurnal and annual ranges of temperature. Broadly, the annual range is a maximum in higher latitudes, with extreme

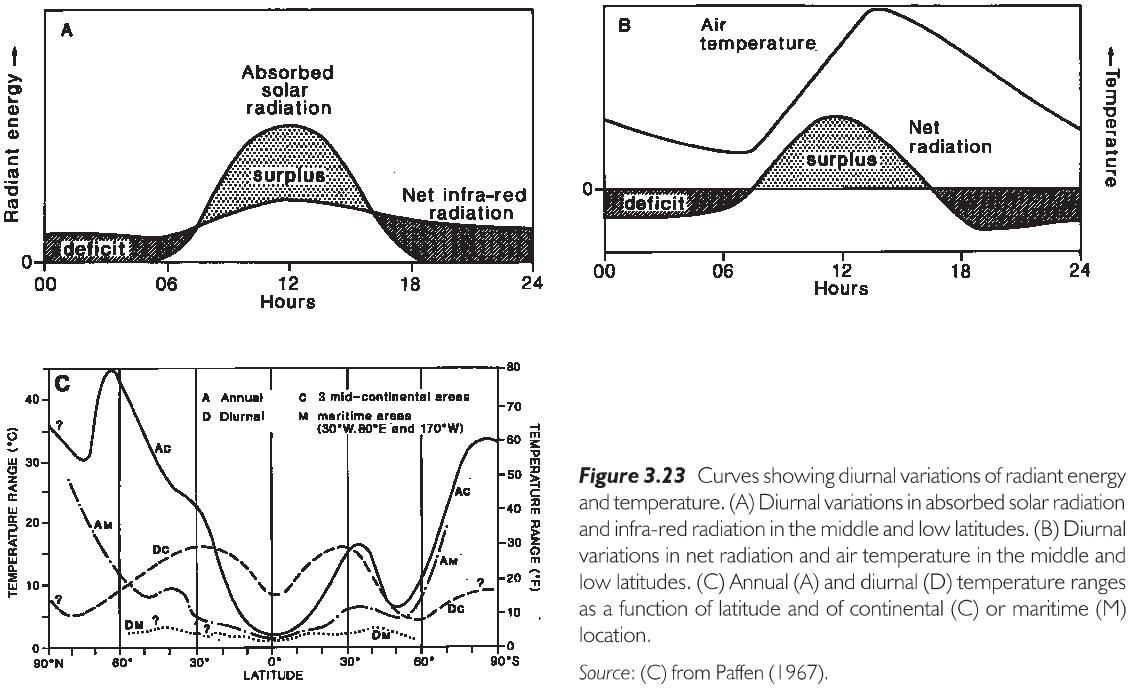

Figure 3.23 Curves showing diurnal variations of radiant energy and temperature. (A) Diurnal variations in absorbed solar radiation and infra-red radiation in the middle and low latitudes. (B) Diurnal variations in net radiation and air temperature in the middle and low latitudes. (C) Annual (A) and diurnal (D) temperature ranges as a function of latitude and of continental (C) or maritime (M) location.

Source: (C) from Paffen (1967).

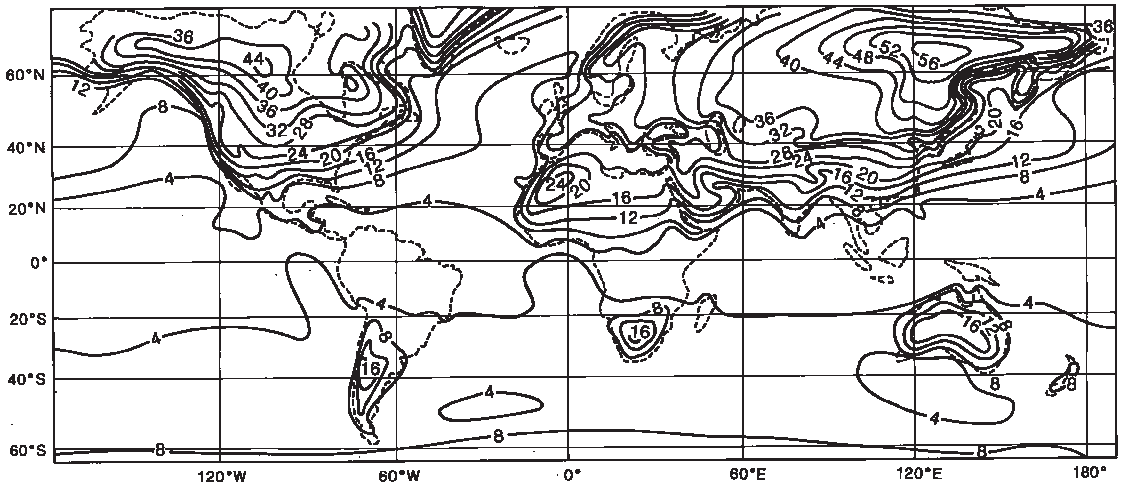

Figure 3.24 The mean annual temperature range (°C) at the earth's surface.

Source: Monin, Crowley and North (1991). Courtesy of the World Meteorological Organization.

values about 65°N related to the effects of continentality and distance to the ocean in interior Asia and North America (Figure 3.24). In contrast, in low latitudes the annual range differs little between land and sea because of the thermal similarity between tropical rainforests and tropical oceans. The diurnal range is a maximum over tropical land areas, but it is in the equatorial zone that the diurnal variation of heating and cooling exceeds the annual one (Figure 3.23C), due to the small seasonal change in solar elevation angle at the equator.

E ATMOSPHERIC ENERGY AND HORIZONTAL HEAT TRANSPORT

So far, we have given an account of the earth's heat budget and its components. We have already referred to two forms of energy: internal (or heat) energy, due to the motion of individual air molecules, and latent energy, which is released by condensation of water vapour. Two other forms of energy are important: geopotential energy due to gravity and height above the surface, and kinetic energy associated with air motion.

Geopotential and internal energy are interrelated, since the addition of heat to an air column not only increases its internal energy but also adds to its geopotential as a result of the vertical expansion of the air column. In a column extending to the top of the atmosphere, the geopotential is approximately 40 per cent of the internal energy. These two energy forms are therefore usually considered together and termed the total potential energy (*PE*). For the whole atmosphere

potential energy $\approx 10^{24}$ J
kinetic energy $\approx 10^{10}$ J

In a later section (Chapter 6C), we shall see how energy is transferred from one form to another, but here we consider only heat energy. It is apparent that the receipt of heat energy is very unequal geographically and that this must lead to great lateral transfers of energy across the surface of the earth. In turn, these transfers give rise, at least indirectly, to the observed patterns of global weather and climate.

The amounts of energy received at different latitudes vary substantially, the equator on the average receiving 2.5 times as much annual solar energy as the poles. Clearly, if this process were not modified in some way the variations in receipt would cause a massive accumulation of heat within the tropics (associated with gradual increases of temperature) and a corresponding deficiency at the poles. Yet this does not happen, and the earth as a whole is approximately in a state of thermal equilibrium. One explanation of this equilibrium could be that for each region of the world there is equalization between the amount of incoming and outgoing radiation. However, observation shows that this is not so (Figure 3.25), because, whereas incoming radiation varies appreciably with changes in latitude, being highest at the equator and declining to a minimum at the poles, outgoing radiation has a more even latitudinal

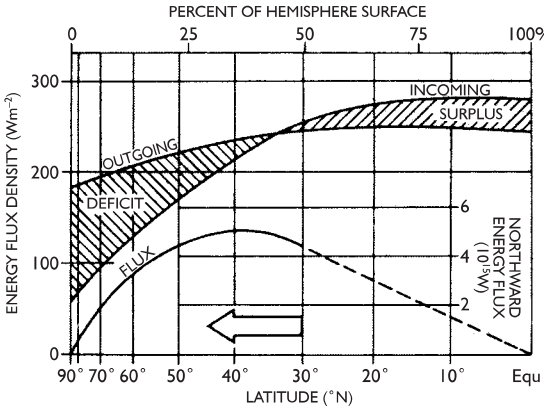

Figure 3.25 A meridional illustration of the balance between incoming solar radiation and outgoing radiation from the earth and atmosphere* in which the zones of permanent surplus and deficit are maintained in equilibrium by a poleward energy transfer.†

Sources: *Data from Houghton; after Newell (1964) and *Scientific American*. †After Gabites.

distribution owing to the rather small variations in atmospheric temperature. Some other explanation therefore becomes necessary.

I The horizontal transport of heat

If the net radiation for the whole earth–atmosphere system is calculated, it is found that there is a positive budget between 35°S and 40°N, as shown in Figure 3.26C. The latitudinal belts in each hemisphere separating the zones of positive and negative net radiation budgets oscillate dramatically with season (Figure 3.26A and B). As the tropics do not get progressively hotter or the high latitudes colder, a redistribution of world heat energy must occur constantly, taking the form of a continuous movement of energy from the tropics to the poles. In this way the tropics shed their excess heat and the poles, being global heat sinks, are not allowed to reach extremes of cold. If there were no meridional interchange of heat, a radiation balance at each latitude would be achieved only if the equator were 14°C warmer and the North Pole 25°C colder than today. This poleward heat transport takes place within the atmosphere and oceans, and it is estimated that the former accounts for approximately two-thirds of the required total. The horizontal transport (*advection* of heat) occurs in the form of both latent heat (that is, water vapour, which subsequently condenses) and sensible

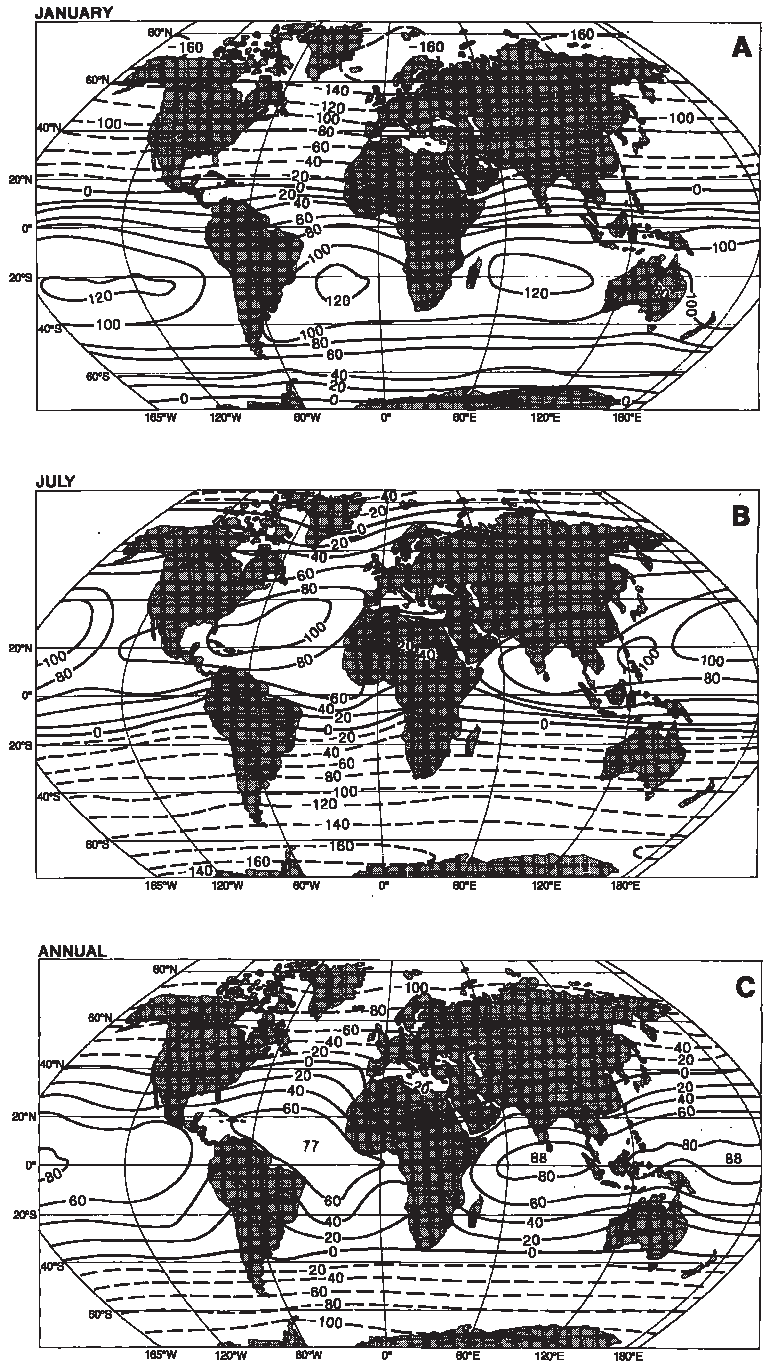

Figure 3.26 Mean net planetary radiation budget (R_n) (W m^{-2}) for a horizontal surface at the top of the atmosphere (i.e. for the earth–atmosphere system). (A) January. (B) July. (C) Annual.

Sources: Ardanuy *et al*. (1992) and Kyle *et al*. (1993). Stephens *et al*. (1981). (A), (B) By permission of the American Geophysical Union. (C) *From Bulletin of the American Meteorological Society*, by permission of the American Meteorological Society.

heat (that is, warm airmasses). It varies in intensity according to the latitude and the season. Figure 3.27B shows the mean annual pattern of energy transfer by the three mechanisms. The latitudinal zone of maximum total transfer rate is found between latitudes 35° and 45° in both hemispheres, although the patterns for the individual components are quite different from one another. The latent heat transport, which occurs almost wholly in the lowest 2 or 3 km, reflects the global wind belts on either side of the subtropical high-pressure zones (see Chapter 7B). The more important meridional transfer of sensible heat has a double maximum not only latitudinally but also in the vertical plane, where there are maxima near the surface and at about 200 mb. The high-level transport is particularly significant over the subtropics, whereas the primary latitudinal maximum of about 50° to 60°N is related to the travelling low-pressure systems of the westerlies.

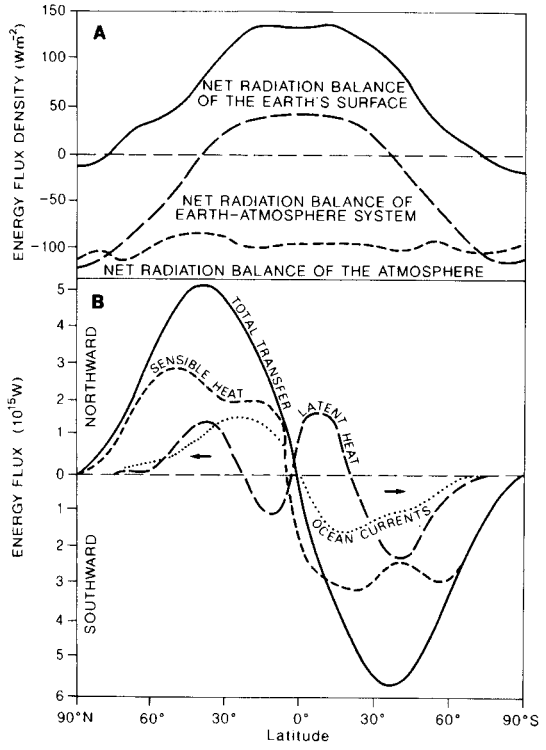

Figure 3.27 (A) Net radiation balance for the earth's surface of 101 W m^{-2} (incoming solar radiation of 156 W m^{-2}, minus outgoing long-wave energy to the atmosphere of 55 W m^{-2}); for the atmosphere of –101 W m^{-2} (incoming solar radiation of 84 W m^{-2}, minus outgoing long-wave energy to space of 185 W m^{-2}); and for the whole earth–atmosphere system of zero. (B) The average annual latitudinal distribution of the components of the poleward energy transfer (in 10^{15} W) in the earth–atmosphere system.

Source: From Sellers (1965).

The intensity of the poleward energy flow is closely related to the meridional (that is, north–south) temperature gradient. In winter this temperature gradient is at a maximum, and in consequence the hemispheric air circulation is most intense. The nature of the complex transport mechanisms will be discussed in Chapter 7C.

As shown in Figure 3.27B, ocean currents account for a significant proportion of the poleward heat transfer in low latitudes. Indeed, recent satellite estimates of the required total poleward energy transport indicate that the previous figures are too low. The ocean transport may be 47 per cent of the total at 30 to 35°N and as much as 74 per cent at 20°N; the Gulf Stream and Kuro Shio currents are particularly important. In the southern hemisphere, poleward transport is mainly in the Pacific and Indian Oceans (see Figure 8.30). The energy budget equation for an ocean area must be expressed as

$$R_n = LE + H + G + \Delta A$$

where ΔA = horizontal advection of heat by currents and G = the heat transferred into or out of storage in the water. The storage is more or less zero for annual averages.

2 Spatial pattern of the heat budget components

The mean latitudinal values of the heat budget components discussed above conceal wide spatial variations. Figure 3.28 shows the global distribution of the annual net radiation at the surface. Broadly, its magnitude decreases poleward from about 25° latitude. However, as a result of the high absorption of solar radiation by the sea, net radiation is greater over the oceans – exceeding 160 W m^{-2} in latitudes 15 to 20° – than over land areas, where it is about 80 to 105 W m^{-2} in the same latitudes. Net radiation is also lower in arid continental areas than in humid ones, because in spite of the increased insolation receipts under clear skies there is at the same time greater net loss of terrestrial radiation.

Figures 3.29 and 3.30 show the annual vertical transfers of latent and sensible heat to the atmosphere. Both fluxes are distributed very differently over land and seas. Heat expenditure for evaporation is at a maximum in tropical and subtropical ocean areas, where it

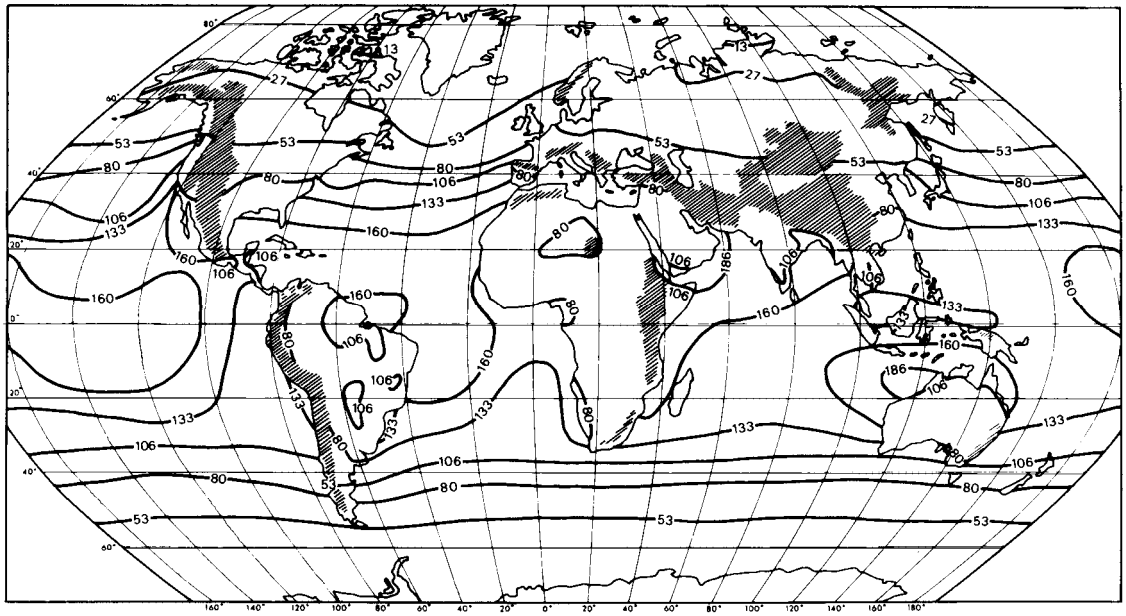

Figure 3.28 Global distribution of the annual net radiation at the surface, in W m^{-2}.

Source: After Budyko *et al*. (1962).

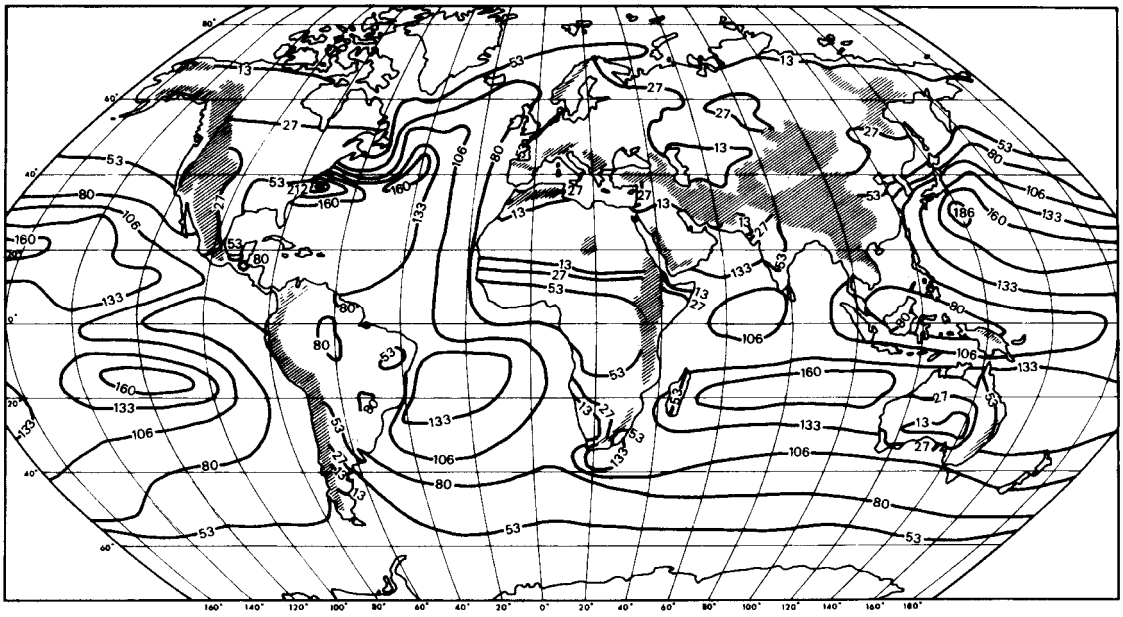

Figure 3.29 Global distribution of the vertical transfer of latent heat, in W m^{-2}.

Source: After Budyko *et al*. (1962).

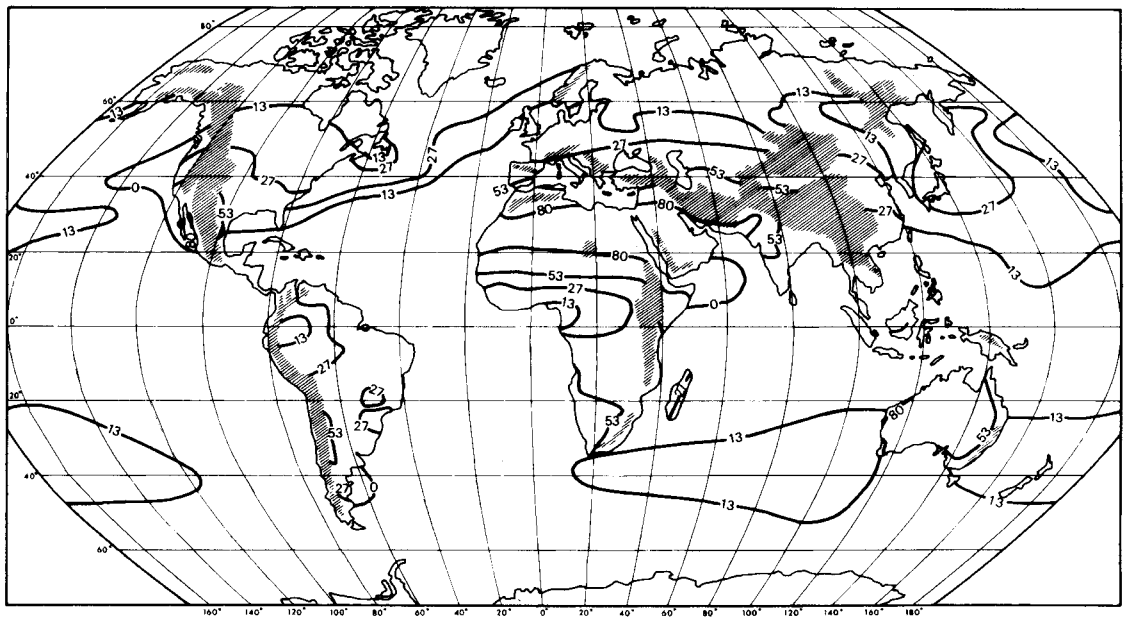

Figure 3.30 Global distribution of the vertical transfer of sensible heat, in W m^{-2}.

Source: After Budyko *et al*. (1962).

exceeds 160 W m^{-2}. It is less near the equator, where wind speeds are somewhat lower and the air has a vapour pressure close to the saturation value (see Chapter 3A). It is clear from Figure 3.29 that the major warm currents greatly increase the evaporation rate. On land, the latent heat transfer is largest in hot, humid regions. It is least in arid areas with low precipitation and in high latitudes, where there is little available energy.

The largest exchange of sensible heat occurs over tropical deserts, where more than 80 W m^{-2} is transferred to the atmosphere (see Figure 3.30). In contrast to latent heat, the sensible heat flux is generally small over the oceans, reaching only 25–40 W m^{-2} in areas of warm currents. Indeed, negative values occur (transfer to the ocean) where warm continental airmasses move offshore over cold currents.

SUMMARY

Almost all energy affecting the earth is derived from solar radiation, which is of short wavelength (<4 μm) due to the high temperature of the sun (6000 K) (i.e. Wien's Law). The solar constant has a value of approximately 1368 W m^{-2}. The sun and the earth radiate almost as black bodies (Stefan's Law, $F = \sigma T^4$), whereas the atmospheric gases do not. Terrestrial radiation, from an equivalent black body, amounts to only about 270 W m^{-2} due to its low radiating temperature (263 K); this is infra-red (long-wave) radiation between 4 and 100 μm. Water vapour and carbon dioxide are the major absorbing gases for infra-red radiation, whereas the atmosphere is largely transparent to solar radiation (the greenhouse effect). Trace gas increases are now augmenting the 'natural' greenhouse effect (33 K). Solar radiation is lost by reflection, mainly from clouds, and by absorption (largely by water vapour). The planetary albedo is 31 per cent; 49 per cent of the extraterrestrial radiation reaches the surface. The atmosphere is heated primarily from the surface by the absorption of terrestrial infra-red radiation and by turbulent heat transfer. Temperature usually decreases with height at an average rate of about 6.5°C/km in the troposphere. In the stratosphere and thermosphere, it increases with height due to the presence of radiation absorbing gases.

The excess of net radiation in lower latitudes leads to a poleward energy transport from tropical latitudes by ocean currents and by the atmosphere. This is in the form of sensible heat (warm airmasses/ocean water) and latent heat (atmospheric water vapour). Air temperature at any point is affected by the incoming solar radiation and other vertical energy exchanges, surface properties (slope, albedo, heat capacity), land and sea distribution and elevation, and also by horizontal advection due to airmass movements and ocean currents.

DISCUSSION TOPICS

- Explain the respective roles of the earth's orbit about the sun and the tilt of the axis of rotation for global climate.
- Explain the differences between the transmission of solar and terrestrial radiation by the atmosphere.
- What is the relative importance of incoming solar radiation, turbulent energy exchanges and other factors in determining local daytime temperatures?
- Consider the role of clouds in global climate from a radiative perspective.
- What effects do ocean currents have on regional climates? Consider the mechanisms involved for both warm and cold currents.
- Explain the concept of 'continentality'. What climatic processes are involved and how do they operate?

FURTHER READING

Books

Barry, R. G. (1992) *Mountain Weather and Climate* (2nd edn), Routledge, London and New York, 402pp.

Budyko, M. I. (1974) *Climate and Life*, New York, Academic Press, 508pp. [Provides ready access to the work of a pre-eminent Russian climatologist.]

Campbell, I. M. (1986) *Energy and the Atmosphere. A Physical–Chemical Approach* (2nd edn), John Wiley & Sons, Chichester, 337pp.

Essenwanger, O. M. (1985) *General Climatology. Vol. 1A. Heat Balance Climatology. World Survey of Climatology*, Elsevier, Amsterdam, 224pp. [Comprehensive overview of net radiation, latent, sensible and ground heat fluxes; units are calories.]

Fröhlich, C. and London, J. (1985) *Radiation Manual*, World Meteorological Organization, Geneva.

Geiger, R. (1965) *The Climate Near the Ground* (2nd edn), Harvard University Press, Cambridge, MA, 611pp.

Herman, J. R. and Goldberg, R. A. (1985) *Sun, Weather and Climate*, Dover, New York, 360pp. [Useful survey of solar variability (sunspots, electromagnetic and corpuscular radiation, cosmic rays and geomagetic sector structure), long- and short-term relations with weather and climate, and design of experiments.]

Hewson, E. W. and Longley, R. W. (1944) *Meteorology, Theoretical and Applied*, Wiley, New York, 468pp.

Miller, D. H. (1981) *Energy at the Surface of the Earth*, Academic Press, New York, 516pp. [Comprehensive treatment of radiation and energy fluxes in ecosystems and fluxes of carbon; many original illustrations, tables and references.]

NASA (nd) *From Pattern to Process: The Strategy of the Earth Observing System*, Vol. III, EOS Science Steering Committee Report, NASA, Houston, Texas.

Sellers, W. D. (1965) *Physical Climatology*, University of Chicago Press, Chicago, IL, 272pp. [Classic treatment of the physical mechanisms of radiation, the budgets of energy, momentum and moisture, turbulent transfer and diffusion.]

Simpkin, T. and Fiske, R. S. (1983) *Krakatau 1883*, Smithsonian Institution Press, Washington, DC, 464pp.

Strahler, A. N. (1965) *Introduction to Physical Geography*, Wiley, New York, 455pp.

Sverdrup, H. V. (1945) *Oceanography for Meteorologists*, Allen & Unwin, London, 235pp. [Classic text.]

Articles

Ahmad, S. A. and Lockwood, J. G. (1979) Albedo. *Prog. Phys. Geog.* 3, 520–43.

Ardanuy, P. E., Kyle, H. L. and Hoyt, D. (1992) Global relationships among the earth's radiation budget, cloudiness, volcanic aerosols and surface temperature. *J. Climate* 5(10), 1120–39.

Barry, R. G. (1985) The cryosphere and climatic change. In MacCracken, M. C. and Luther, F. M. (eds) *Detecting the Climatic Effects of Increasing Carbon Dioxide*, DOE/ER-0235, US Department of Energy, Washington, DC, pp. 109–48.

Barry, R. G. and Chambers, R. E. (1966) A preliminary map of summer albedo over England and Wales. *Quart. J. Roy. Met. Soc.* 92, 543–8.

Beckinsale, R. P. (1945) The altitude of the zenithal sun: a geographical approach. *Geog. Rev*. 35, 596–600.

Berger, A. (1996) Orbital parameters and equations. In Schneider, S. H. (ed.) *Encyclopedia of Climate and Weather*, Vol. 2, New York, Oxford University Press, pp. 552–7.

Budyko, M. I., Nayefimova, N. A., Aubenok, L. I. and Strokhina, L. A. (1962) The heat balance of the surface of the earth. *Soviet Geography* 3(5), 3–16.

Currie, R. G. (1993) Luni–solar 18.6 and solar cycle 10–11 year signals in U.S.A. air temperature records. *Int. J. Climatology* 13, 31–50.

Foukal, P. V. (1990) The variable sun. *Sci. American* 262 (2), 34–41.

Garnett, A. (1937) Insolation and relief. *Trans. Inst. Brit. Geog*. 5 (71pp.).

Henderson-Sellers, A. and Wilson, M. F. (1983) Surface albedo data for climate modeling. *Rev. Geophys. Space Phys*. 21(1), 743–78.

Kiehl, J. T. and Trenbreth, K. E. (1997) Earth's annual global mean energy budget. *Bull. Amer. Met. Soc.* 78, 197–208.

Kraus, H. and Alkhalaf, A. (1995) Characteristic surface energy balances for different climate types. *Int. J. Climatology* 15, 275–84.

Kung, E. C., Bryson, R. A. and Lenschow, D. H. (1964) Study of a continental surface albedo on the basis of flight measurements and structure of the earth's surface cover over North America. *Mon. Weather Rev*. 92, 543–64.

Kyle, H. L. *et al*. (1993) The Nimbus Earth Radiation Budget (ERB) experiment: 1975–1992. *Bull. Amer. Met. Soc*. 74, 815–30.

Lean, J. (1991) Variations in the sun's radiative output. *Rev. Geophys*. 29, 505–35.

Lean, J. and Rind, D. (1994) Solar variability: implications for global change. *EOS* 75(1), 1 and 5–7.

London, J., Warren, S. G. and Hahn, C. J. (1989) The global distribution of observed cloudiness – a contribution to the ISCCP. *Adv. Space Res*. 9, 161–5.

Lumb, F. E. (1961) *Seasonal variation of the sea surface temperature in coastal waters of the British Isles*. Sci. Paper No. 6, Meteorological Office, HMSO, London (21pp.).

McFadden, J. D. and Ragotzkie, R. A. (1967) Climatological significance of albedo in central Canada. *J. Geophys. Res.* 72(1), 135–43.

Minami, K. and Neue, H-U. (1994) Rice paddies as a methane source. *Climatic Change* 27, 13–26.

Newell, R. E. (1964) The circulation of the upper atmosphere. *Sci American* 210, 62–74.

Paffen, K. (1967) Das Verhältniss der Tages – zur Jahreszeitlichen Temperaturschwankung. *Erdkunde* 21, 94–111.

Ramanathan, V., Barkstrom, B. R. and Harrison, E. F. (1990) Climate and the earth's radiation budget. *Physics Today* 42, 22–32.

Ramanathan, V., Cess, R. D., Harrison, E. F., Minnis, P., Barkstrom, B. R., Ahmad, E. and Hartmann, D. (1989) Cloud-radiative forcing and climate: results from the Earth Radiation Budget Experiment. *Science* 243, 57–63.

Ransom, W. H. (1963) Solar radiation and temperature. *Weather* 8, 18–23.

Sellers, W. D. (1980) A comment on the cause of the diurnal and annual temperature cycles. *Bull. Amer. Met. Soc*. 61, 741–55.

Stephens, G. L., Campbell, G. G. and Vonder Haar, T. H. (1981) Earth radiation budgets. *J. Geophys. Res*. 86(C10), 9739–60.

Stone, R. (1955) Solar heating of land and sea. *J. Geography* 40, 288.

Strangeways, I. (1998) Back to basics: the 'met. enclosure'. Part 3: Radiation. *Weather* 53, 43–9.

Tully, J. P. and Giovando, L. F. (1963) Seasonal temperature structure in the eastern subarctic Pacific Ocean. In Dunbar, M. J. (ed.) *Maritime Distributions, Roy. Soc. Canada, Spec. Pub*. 5, 10–36.

Weller, G. and Wendler G. (1990) Energy budgets over various types of terrain in polar regions. *Ann. Glac.* 14, 311–14.

Wilson, R. C. and Hudson, H. S. (1991) The sun's luminosity over a complete solar cycle. *Nature* 351, 42–3.